JPRS L/10159

3 December 1981

Worldwide Report

TELECOMMUNICATIONS POLICY, RESEARCH AND DEVELOPMENT

(FOUO 17/81)

FBIS FOREIGN BROADCAST INFORMATION SERVICE

NOTE

JPRS publications contain information primarily from foreign newspapers, periodicals and books, but also from news agency transmissions and broadcasts. Materials from foreign-language sources are translated; those from English-language sources are transcribed or reprinted, with the original phrasing and other characteristics retained.

Headlines, editorial reports, and material enclosed in brackets [] are supplied by JPRS. Processing indicators such as [Text] or [Excerpt] in the first line of each item, or following the last line of a brief, indicate how the original information was processed. Where no processing indicator is given, the information was summarized or extracted.

Unfamiliar names rendered phonetically or transliterated are enclosed in parentheses. Words or names preceded by a question mark and enclosed in parentheses were not clear in the original but have been supplied as appropriate in context. Other unattributed parenthetical notes within the body of an item originate with the source. Times within items are as given by source.

The contents of this publication in no way represent the policies, views or attitudes of the U.S. Government.

APPROVED FOR RELEASE: 2007/02/09: CIA-RDP82-00850R000400080013-5

JPRS L/10159

3 December 1981

WORLDWIDE REPORT

TELECOMMUNICATIONS POLICY, RESEARCH AND DEVELOPMENT

(FOUO 17/81)

CONTENTS

USSR

Integrated Istok Analog-Digital Communications System Test Results
(L. Ya. Misulovin, et al.; ELEKTROSVYAZ', Sep 81)..... 1

WEST EUROPE

ITALY

Equipment Used at Rai Mt. Venda Transmitting Station
(Giulio Paolo Pacini; ELETTRONICA E TELECOMUNICAZIONI, May-Jun 81)..... 14

Silicon Avalanche Photodetector for Optical Communications
(M. Conti, et al.; ELETTRONICA E TELECOMUNICAZIONI, May-Jun 81)..... 48

USSR

UDC 621.395.345.3

INTEGRATED ISTOK ANALOG-DIGITAL COMMUNICATIONS SYSTEM TEST RESULTS

Moscow ELEKTROSVYAZ' in Russian No 9, Sep 81 (manuscript received 13 May 80)
pp 4-10

[Article by L.Ya. Misulovin, V.V. Makarov and Yu.A. Baklanov: "Test Results of the Integrated Analog and Digital Communications System: the 'Istok' Analog and Digital Unified Communications Network"]

[Text] The development of the first analog and digital communications system with centralized control within the bounds of a network section has been completed in the USSR and the nations of socialist cooperation, where this system is called the "unified (for the USSR and GDR) analog-digital communications system", the "Istok" YeSS ATs. The system design is the result of the cooperation of two CEMA member nations: the USSR and GDR. The major switching components, basic circuits and software were developed by USSR specialists while the GDR specialists designed the basic structure, including the connectors, operational process fundamentals and designer documentation for the control complex.

Two test regions were set up to conduct thorough tests of the unified analog-digital communications system equipment: in the Istrinskiy rayon of the Moskovskaya oblast and in Berlin. Both regions were created through the joint efforts of USSR and GDR enterprises. The alignment and testing of the equipment in the Istrinskiy test region were performed by USSR specialists, while in the Berlin region, it was done by USSR and GDR specialists.

The tests of both zones were completed at the beginning of 1980. The results of the tests made it possible to correct the design documentation for the sytem and turn it over for industrial production in the USSR and GDR, as well as work out the system program software for series production and work up the operational documentation. But getting the "Istok" YeSS ATs in series production also poses new problems: the creation of a single programming center and a center for training operational personnel.

The successful completion of tests of the Istrinskiy test zone of the "Istok" YeSS ATs is the result of the self-sacrificing labor of equipment designers and specialists of the Istrinskiy RUS (regional communications center).

Work is now underway on the utilization of the "Istok" YeSS ATs as a municipal ATS [automatic telephone exchange], for which the maximum capacity of the system is being expanded up to 8,000 - 10,000 numbers.

The first industrial models of the "Istok" YeSS ATs will be installed in the Ogre RUS of the Latvian SSR (Liyelvarde) and in Saratov.

The Organization of the Istrinskiy Test Zone. The structural configuration of the Istrinskiy test zone communications network of the unified analog-digital communications system is shown in Figure 1; the zone is inscribed within the bounds of the existing telephone network. The unified analog-digital communications system test zone, just as all rural telephone networks (STS), is designed on a radial junction center principle; included in it were the key exchange, OPS (type 1) and three terminal exchanges OS1 - OS3 (type 3). The key exchange was incorporated as a central exchange while the OS1 - OS3 exchanges were included as terminal offices. In order to assure completeness of the tests, the key exchanges of the test zone, in contrast to the key office of a conventional rural telephone network, has a direct output to the regional ATS's and AMTS's [automated long-distance telephone exchanges] of Moscow.

Several junction line (SL) trunk groups were set up between the central exchange and the key exchanges. The OS1 [terminal exchange 1] was connected to the key exchange via physical junction lines (FSL), and a common control channel, OKU-FSL, was set up to form the remote control system for OS1 via two two-wire physical junction lines. The OS2 and OS3 terminal offices were connected to the key exchange via IKM [PCM, pulse code modulation] channels, where two channels were used in both cases to check the stand-by system. Linear PCM channels were set up using the "Zona" equipment, where the IKM-30 transmission system was used as the terminal stations.

All of the call routings which were set up in the communications network of Figure 1 are indicated in Table 1. As can be seen from the table, 48 different call routings were established in all. We note that the control of all calls, as well as the offering of additional services (DVO) and all technical operations (TER) were accomplished under the control of the central control unit (TsUU), installed at the key exchange. It was necessary to design program software (PO) with a volume of 200 Kbytes for the central control unit to realize all of the functions enumerated above.

Supplemental kinds of services were made available to subscribers in the test zone, which are shown in Table 2. The types of technical operations realized in the test zone, as well as brief description of their contents, are given in Table 3.

A block diagram of the prototype exchanges for the unified analog and digital communications system which were installed in the Istrinskiy zone is shown in Figure 2 with the equipment indicated, which was housed in more than 20 bays. The following symbols are used in the drawing:

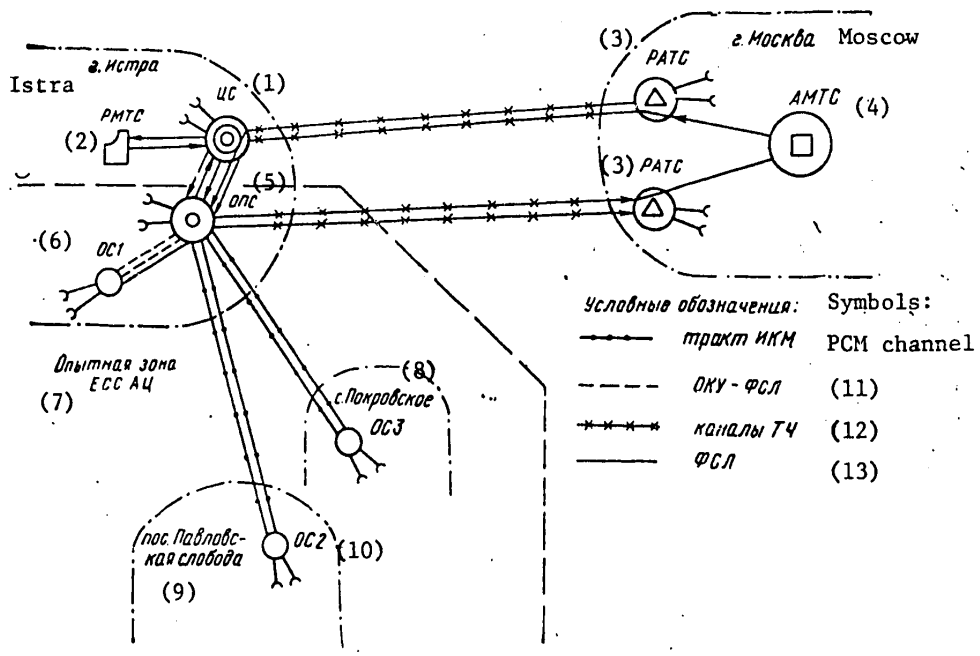

Figure 1.

Key: 1. TsS = central office;
2. RMTS = regional long distance exchange;
3. RATS = regional automatic telephone exchange;
4. AMTS = automatic long distance telephone exchange;
5. OPS = key telephone exchange;
6. OS1 = terminal exchange 1;
7. Test zone of the analog-digital unified communications system;
8. Pokrovskoye village, OS3 [terminal exchange 3];
9. Settlement of Pavlovskaya Sloboda;
10. OS2 = terminal exchange 2;
11. Common control channel for physical junction lines;
12. Voice frequency telegraphy channels;
13. Physical junction lines.

АК [AK] - subscriber sets which serve for the subscriber line loop;

АЛ [AL] - subscriber line;

АЦО [ATsO] - the analog-digital equipment of the IKM-30 transmission system;

БАЛ [BAL] - block of subscriber lines; the switching equipment to which a subscriber line is connected; intended primarily for concentrating (compressing) the telephone load;

БКК [BKK] - the set connection unit for connecting service sets which are busy only in the stage of making a call connection to junction line sets, which are occupied both during the stage of making a call connection and during the conversation;

БОЛТ [BOLT] - terminal line channel unit of the "Zona" equipment; the line signal repeater, remote power supply for unattended repeaters and service intercom system are installed in it;

БСЛ [BSL] - junction line block; the connection equipment to which the junction line sets and service sets of various kinds are connected; it serves to provide access to the trunk groups for various instruments;

КАТ [KAT] - subscriber call fee determination set, intended for transmitting the call fee pulses to meters installed at the subscriber;

ККС [KKS] - conference call unit to provide for a joint conversation with up to eight conference participants;

КСЛ [KSL] - junction line set, which powers the subscriber microphone in the case of an external call (with respect to the exchange in which the subscriber is incorporated);

КСЛВ3 КСЛИ3 [KSLV3, KSLI3] - junction line sets (incoming and outgoing three-wire units) serve for the transmission and reception of interaction signals with an electromechanical automatic telephone exchange;

КС-ПТН [KS-PTN] - switching system for the connection of the tonal dialing receiver (PTN) to the service set (SK); the necessity for it is due to the fact that the time the PTN is occupied is less than the time that SK is occupied;

ОКУ-ФСЛ [OKU-FSL] - The common control channel for physical junction lines; the direct and back-conversion of the control signals transmitted in both directions between the key exchange and terminal exchange 1 are accomplished in it: a series quasi-ternary code into the line and a parallel two-level "one of four" code in the direction of the exchange;

ПТН [PTN] - the touch tone dialing receiver which serves for receiving the touch tone dial signals for a number from a telephone set with a touch tone keyboard;

ПУУ [PUU] - the peripheral controller for interfacting the high speed central control unit to the relatively slow switching equipment;

СК [SK] - a service set, used in the process of making a call connection between an exchange and a subscriber line; it feeds out the tone and ringing signal and receives the ten-step code dialing signals;

СКГ [SKG] - DC service complex, which serves for transmitting and receiving DC signals and is used in the process of establishing call connection of an exchange with a junction line;

СКЧ [SKCh] - the same as the SKG, but only for frequency [AC] signals;

УК [UK] - the control complex - the central controller for the entire analog-digital unified communications system;

УСК1 [USK1] - channel interface; the direct and back-conversion of "time--space" type digital signals are accomplished in it: time multiplexing of the individual channels is provided in the direction of the channel end and spatial multiplexing is provided in the section of the BSL [junction line connection block]; in both cases the signals are digital. Moreover, the USK1 performs the functions of a common control channel via the PCM channel (OKU-IKM); in this case, the control instructions undergo direct and back "series-parallel" conversion: in the direction of the PUU [peripheral control unit], the instruction is represented by a parallel code and in the direction of the line channel, by a series code;

УСК2 [USK2] - the same as USK1, but without the function of the common control channel via the PCM channel;

УСК3 [USK3] - the same as the USK1, but without the "time--space" conversion function;

ШК [ShK] - the patch cord equipment, intended for powering the microphones of the calling and called subscribers in the case of call connections within an exchange.

The operational principle of this communications system is described in [1].

TABLE 1

Сторона	Сеть	Станция	INCOMING END: 4 ОПС	5 ОС1	6 ОС2	7 ОС3	8 ЦС	(1) Существ. сеть г. Истры: РМТС (9)	(2) Моск. сеть: РАТС (10)	(3) Межгор. сеть: АМТС (11)
OUTGOING END	YeSS ECC ATs	4 ОПС	+	+	+	+	+	□	+	+
		5 ОС1	+	+	○	○	○	◇	○	○
		6 ОС2	+	○	+	○	○	◇	○	○
		7 ОС3	+	○	○	+	○	◇	○	○
Исходящая	(1) Существ. сеть г. Истры	ЦС (8)	+	○	○	○	–	–	–	–
		РМТС (9)	□	◇	◇	◇	–	–	–	–
	(2) Моск. сеть	РАТС (10)	□	◇	◇	◇	–	–	–	–
	(3) Межгор. сеть	АМТС (11)	□	◇	◇	◇	–	–	–	–

Symbols used: "+" are for a direct connection;
Circles: the call connection passes through the key exchange;
Squares: the call connection passes through the central office;
Diamonds: the call connection passes through the key exchange and the central office;
Dashes: the call connections which were not incorporated in the test program.

[Key to Table 1]:

1. Existing network of Istra;
2. Moscow;
3. Long distance network;
4. OPS [key exchange];
5. OS1 [terminal exchange 1];
6. OS2;
7. OS3;
8. TsS [central office];
9. RMTS [regional long distance telephone exchange];
10. RATS [regional automatic telephone exchange];
11. AMTS [automatic long distance telephone exchange].

The tests of the "Istok" prototype were broken down into three stages, each of which had its own program and testing procedure:

--The line tests, during which the operability of the system when making individual call connections was checked and the electrical parameters of the speech channel were measured;

--Experimental operation with the simulation of a subscriber load, which was created by the staff workers performing the tests; the task of this stage was to check the operational capability of the test zone under dynamic conditions;

--Test operation with actual subscriber. In this stage, 94 telephone sets were connected to the key telephone exchange, 52 sets to OS1 [terminal exchange 1], 17 sets to OS2 and 17 sets to OS3; 180 telephone sets were connected in all. Because of the incomplete utilization of the installed subscriber capacities during trial operation with actual subscribers, a supplemental subscriber load was produced with test telephone sets designed so as to bring the overall load up to six to eight calls per day per installed telephone set. The task of this stage was to check the operational stability of the equipment with long term exposure to the actual load.

The functioning of all components and the system as a whole was checked during the line testing stage; the electrical measurements confirmed the high quality of the speech channel.

Despite the positive results of the line tests, a whole series of characteristic defects were found in the trial operational stage with the simulation of the subscriber load, where these defects were immediately eliminated. The following are to be numbered among them:

In the program software: the initiation of the search program cycles for trunk routes (SP) with the overflow of the common memory field; "hanging-up" calls because of errors in the SP search program; "hanging-up" calls when the servicing

TABLE 2

Item No.	Designation of the Service	Brief Description of Service Contents
1	Conference calling	Makes it possible to hold a conference between three to eight participants, including the caller setting it up.
2	Call transfer to another telephone set (TA)	Permits the subscriber to order his own telephone to transfer a call to another telephone when he is absent
3	Stand-by with return call-up	Permits placing the calling subscriber on hold when the called subscriber is busy. After the latter is cleared, the calling subscriber is first called, and after his answer, then the called subscriber. During the holding time, the calling subscriber can make outgoing and receive incoming calls.
4	Abbreviated number dialing	Makes it possible for the subscriber to call subscribers of local, zonal and long-distance networks by means of dialing an abbreviated number.
5	Call without number dialing	Makes it possible to call a subscriber of a local, zonal or long distance network without dialing the number by means of taking the receiver off the hook.
6	Transfer of a call connection to another subscriber	Makes it possible for subscriber A (or B), who is having a conversation with subscriber B (or A), to connect subscriber B (or A) with subscriber C, in this case, eliminating himself from the call.
7	Obtaining information during a conversation	Permits subscriber A, who is having a conversation with subscriber B, to call up subscriber C, and after obtaining the the information, return to the interrupted conversation with subscriber B.
8	Inhibiting incoming calls for an indicated period of time	Permits a subscriber to temporarily block incoming calls from all subscribers until the time stipulated in the order expires.

TABLE 3

Item No.	Kind of Technical Operations	Brief Description of the Contents of the Technical Operations
1	Call fee determination	Metering local conversations (the number of them) in centralized counters (in the memory of the central control unit) and in meters installed at the subscriber
2	Statistics	Gathering data on the number of calls which came in and the number of conversations which took place
3	Technical servicing	Monitoring the operability and diagnosing faults in sets which participate in making a call connection, as well as in the switching system, peripheral controllers, subscriber lines and the control complex
4	Operator communications with the system	Feeding messages to the operator concerning the failure of individual devices or defective situations (failures) during the time a call is handled . Operator actions during technical servicing are: feeding punched tapes and out in real time, blocking and releasing functional devices, analyzing the status of main frame memory data files on the handling of calls, feeding out data on a change in the category of subscriber lines.

remand register (RTO) overflows because of errors in the analysis programs; "hanging-up" subscriber sets in the oriented check memory in the case of outgoing calls because of errors in the external outgoing traffic programs; false registering of failures in the PUU's [peripheral control units] because of interference in the scanning matrix and inadequate reliability of the programs for timely monitoring of the operational capability.

In the hardware: a change in the number of channels connected to the speech channel (pulse code modulation), on the operation of the OKU [common control channel]; incorrect connection and disconnection of equipment participating in establishing call connections because of unstable operation of the PUU programmers of the OS1--OS3 terminal exchanges; incorrect connection and disconnection of equipment participating in making call connections because of the generation of "false" control data for the common control channel. Failures of certain peripheral control unit circuits of the OS1--OS3 terminal exchanges with repeated interruptions in the primary mains voltage (220 volts).

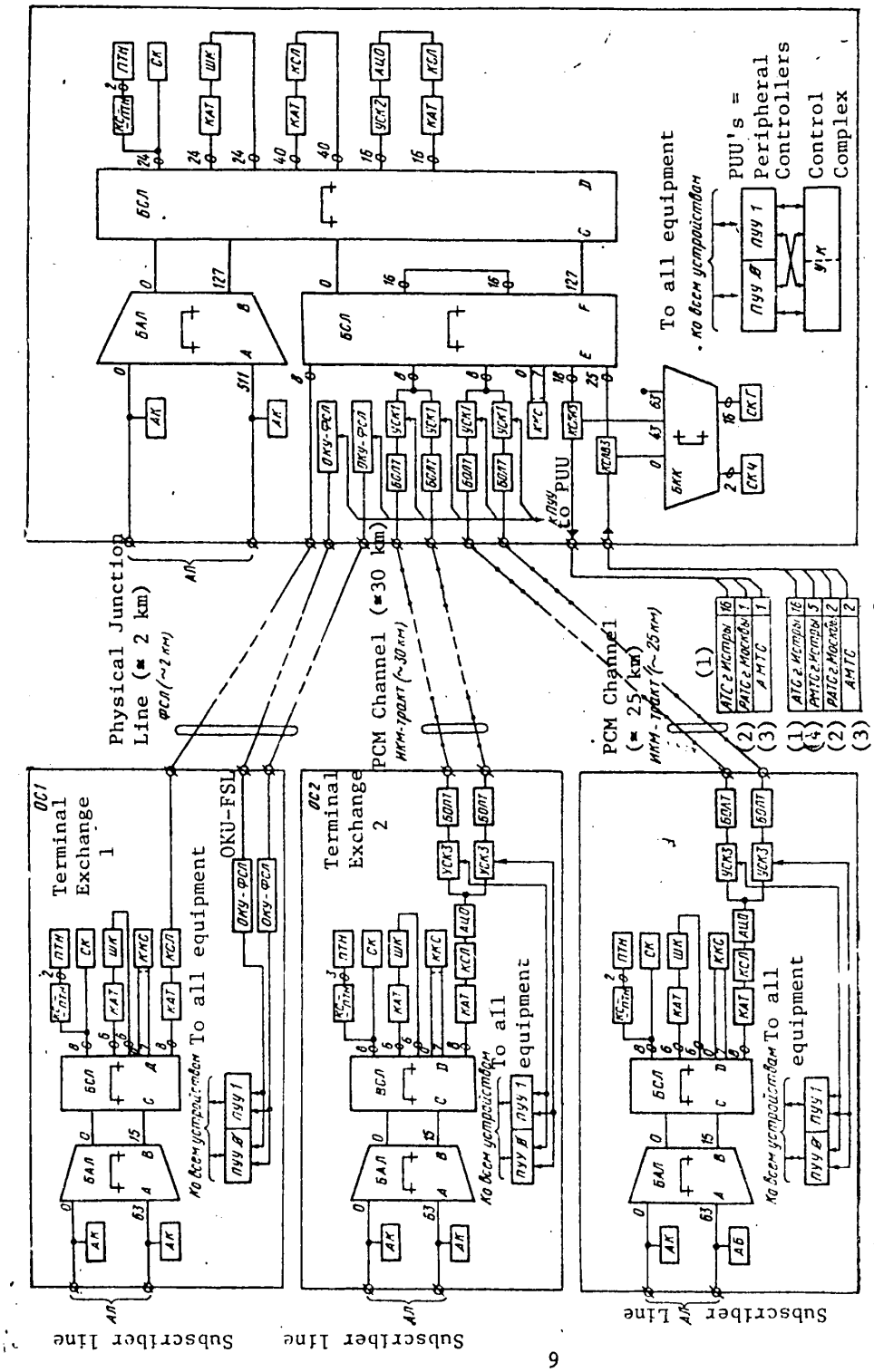

Figure 2.

Key: 1. Istra automatic telephone exchange;
2. Moscow regional automatic telephone exchange;
3. Automatic long distance telephone exchange;
4. Istra regional long distance telephone exchange.

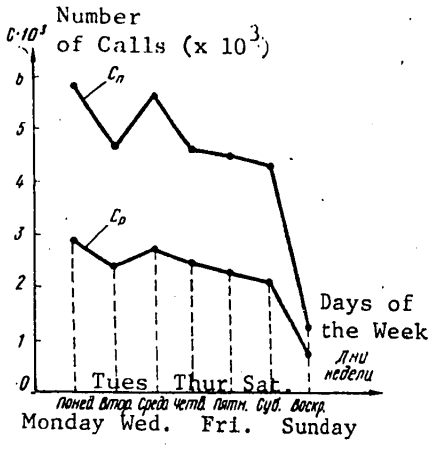

Figure 3.

Key: C_{Π} = total number of calls made;
C_p = number of calls ending in a conversation.

After the defects enumerated above were eliminated, the number of call failures for technical reasons dropped down to 0.3--0.5 percent.

Some 171,000 call connections were made in the trial operational stage with real subscribers; of them, 50 to 55 percent of the calls ended in a conversation. The distribution of the overall number of calls C_{Π} and the number of calls ending in a conversation, C_p, is shown in Figure 3 as a function of the days of the week. Two peak load hours were found for the key exchange during a 24 hour day; from 9:30 to 10:30 AM and from 2:30 to 3:30 PM with the calls numbering 600 to 700.

During the trial operation period, which lasted for several months, 28 complaints came in from subscribers. The reason for the complaints were: 20 because of programming errors; 3 because of damage to the cable within the exchange; 4 because of failures in subscriber lines; and 1 was the fault of technical personnel. Over this same time period, there were 30 short term interruptions (of 2 to 3 minutes) in handling calls with the setting of the exchanges to the initial state. The reasons for their occurrence were: 25 percent were the fault of technical personnel; 15 percent were because of data dropouts in the memories (ZU), since a portion of the memory capacity had no back-up; 20 percent were because of a lack of software for the selective, facility by facility setting of individual exchanges to the initial state; and 40 percent were because of programming errors.

Thus, despite the fact that the first two stages of tests of the exchange in the trial zone yielded positive results, defects continued to be found in its program software. Moreover, there were failures in six pieces of hardware, where three of the failed units were detected by automatic monitors, while three more were found following test calls.

During the trial operation with an actual subscriber load, the operational quality of the exchange equipment in the test zone was checked periodically by means of making test calls. The results of these tests are given in Table 4. In this case, unsuccessful attempts to make a call occurred for unknown reasons only in the case of outgoing and incoming calls from telephone sets in the Istra automatic telephone exchange.

Trial operation of the "Istok" YeSS ATs demonstrated the reliable operation of the major system equipment. Thus, in the course of two years from the moment the factory tests were completed until the end of trial operation, there were no faults in 363 integrated selector switches (MIS), with the exception of those cases, the reasons for which were errors in the operation of other parts of the system, in

TABLE 4

Test Calls in the Course of an Hour			
Total Number of Attempts	Successful (Ending in a Conversation)	Unsuccessful	
		For Known Technical Reasons	For Unknown Technical Reasons
1,200	1,191	5	4
1,000	990	4	6
1,200	1,188	6	6

particular, software errors. The YeFS [not further defined] connectors produced by the GDR proved to be just as reliable. The control unit for the analog-digital unified communications system produced by the "Robotron" combine during the testing period from June to December of 1979, as well as up to the present time, did not have a single flaw.

It should be noted that following the elimination of the bulk of the program errors, the trial zone operated better when there were either no operational personnel at all or the personnel were of the intermediate skill level, since the highly skilled workers (designers), having confidence in their own knowledge, did not always intervene in system operation with justification, something which causes additional short term interruptions in system service which were noted above (25 percent of the cases).

The Berlin Test Zone. To check the operational performance of the analog-digital unified communications system under actual GDR telephone network operating conditions, a test zone for the analog-digital unified communications system was set up in Berlin, which was practically analogous to the Istrinskaya zone (one key exchange and three terminal exchanges). This zone was tied into the Berlin telephone network, and internal, local, long distance and international calls were made with it. In all, more than 300 subscribers were connected to the Berlin zone exchanges.

During the time of trial operation of the system, the overall losses in the case of internal communications amounted to 2.2 percent. This loss level drops off to 0.6 percent (similar to the Istrinskaya zone), if losses are excluded which are related to program errors which were found. The overall losses for the case of external service amounted to 1.9 percent.

Among the call connections which were made in the Berlin test zone, it is interesting to note the international ones, where the subscribers of the trial zone of the analog-digital unified communications system in Berlin were automatically connected via the international telephone network to the analog-digital unified communications system test zone subscribers in Istra in the Moscow oblast.

The trial operation of the Berlin test zone which was carried out at the start of 1980 went successfully.

Technical Economic Indicators of the Analog-Digital Unified Communications System. The "Istok" YeSS ATs has a number of special features and unique differences from well known foreign communications systems, which extend its capabilities and improve its economy:

--The system can operate both with autonomously controlled quasi-electronic automatic telephone exchanges and with the key exchange of an integrated communications system with centralized control within the bounds of a communications network section;

--It can switch both analog and digital signals without the forced conversion from one form to the other (for switching purposes);

--Remotely controlled terminal stations can be connected to the key office both via PCM channels and physical junction lines;

--The system has a custom designed integrated selector switch;

—It does not require air conditioning, forced ventillation or false floors;

--The system is put together using elements and technology available in the USSR and the GDR.

--As compared to a communications network equipped with crossbar automatic telephone exchanges and transmission systems with frequency multiplexing of the channels, the communications network organized with the "Istok" analog-digital unified communications system has the following advantages: the overall volume of equipment and area occupied by it are reduced; the process of technical operation has been automated and centralized, something which is accompanied by a reduction of several times in the operational labor intensity; the quality of the speech channel and the carrying capacity of the system have been sharply increased; its reliability has risen sharply while the number of faults has been reduced; subscribers are offered additional kinds of service; the possibility of transmitting digital data at a high confidence level is provided; the products list of equipment has been reduced, and the throughput per unit of production area has increased.

It should be noted that all of the advantages of "Istok" YeSS ATs exchanges can be fully utilized in an integrated mode if a PCM transmission system and primary power supplies for the terminal stations adapted to these exchanges will be designed.

International Approval. A working exhibition model of the analog-digital unified communications system [2] was constructed in a short period of time by GDR enterprises working from corrected documentation; this prototype was successfully exhibited at the "Telcom-79" international exhibition in Geneva. This same prototype was exhibited at the Leipzig spring fair in March of 1980. In this case,

the results of the tests in the Istrinskiy and Berlin test zones were already taken into account in the documentation from which this prototype was constructed.

A control complex developed jointly by USSR and GDR specialists is used as the central control unit in the "Istok" YeSS ATs. A prototype of the control unit for the analog-digital unified communications system (UK 4310) was built in the GDR "Robotron" combine. It was exhibited at the international exhibition devoted to the 30th anniversary of the CEMA, which was held in Moscow in June of 1979, after which it was used to conduct the tests in the Istrinskiy test zone.

BIBLIOGRAPHY

1. "Integral'naya kvazielektronnaya analogo-tsifrovaya sistema svyazi - IKE ATsSS" ["An Integrated Quasielectronic Analog and Digital Communications System, the IKE ATsSS"], ELEKTROSVYAZ' [ELECTRICAL COMMUNICATIONS], 1975, Nos. 10, 11.

2. Tietze P., "Demonstrations-muster von Einrichtungen einer ENSAD Ortszentrale" ["Demonstration Model of the Equipment of an Analog and Digital Unified Communications System Local Central Office"], FERNMELDETECHNIK [COMMUNICATIONS ENGINEERING], 1979, No. 5.

8225
CSO: 8344/0140

ITALY

EQUIPMENT USED AT RAI MT. VENDA TRANSMITTING STATION

Turin ELETTRONICA E TELECOMUNICAZIONI in Italian May-Jun 81 pp 98-114

[Article by Giulio Paolo Pacini*: "Combining Units for FM Broadcasting Transmitters --Equipment for the Mt Venda Transmitting Center"]

[Text] Summary--Combining Units for FM Broadcasting Transmitters (Equipment for the Transmitting Center of Mt Venda)--This paper deals with a general description of the operation of a combining unit for frequency-modulated broadcasting transmitters, and of the structure of distributed constant circuits which are the most appropriate for the implementation of these combiners. Moreover, it presents some examples of prototypes, designed and set up at the RAI Research Center, which have been manufactured in a small mass-production for the RAI transmitting equipment. Particular attention is given to one prototype implemented, as a unique model, in the Transmitting Center of Mt Venda: it represents a significant example because of the particular problems its design has posed, owing to the small percent distance between adjacent frequencies in the transmitters, as well as to their high power.

1. General Remarks

The FM radio programs transmitted by RAI in the 87.5-104 MHz band and radiated by a transmitting center or by a bounce repeater are generally three and in some cases four in number. They are normally radiated by a single wide-band antenna and not by various separate antennas; this is because of the costs of the big transmitting antennas, the power cables and installation, the space taken up in relation to the gain and the solution of other, collateral problems.

The radiation of several programs from a single antenna requires the use of a combining unit that has the task of combining the power of various transmitters in a single antenna cable, with proper insulation maintained between the transmitters connected to the unit.

In addition, the combining unit must offer good adaptation of impedance to the transmitters; it must not introduce considerable power losses off the carrier or off

---

* Doctor of Engineering Giulio Paolo Pacini of the Research Center of RAI [Italian Radio Broadcasting and Television Company]-Turin.

Typescript received 12 March 1981.

the side bands, and it must not introduce into the signal in transit considerable distortions of phase and amplitude, that would be found in the demodulated low-band stereophonic signal in the form of harmonic distortion, intermodulation, linear and nonlinear diaphony, improper amplitude/frequency response.

2. Description of Several Combining Cirucits for FM Transmitters

The circuits that make it possible to combine two or more FM transmitters can be constructed in several ways, depending on the characteristics of the installation, the number and power of the transmitters, and especially, the gap between two contiguous carriers. They break down fundamentally into two groups: star circuit, and ring circuit with hybrids.

2.1. Star Circuit

The basic diagram is as indicated in Figure 1 for the case of three transmitters. These feed three lines that converge at a common point S (the center of the star), to whcih the antenna cable is also connected. From each of the three lines is shunted, at a quarter-wave from point S, a filtering network F with passband characteristic: it presents high impedance at the frequencies of the transit channel, and very low impedance--and therefore high attenuation--at the frequencies of the other two channels.

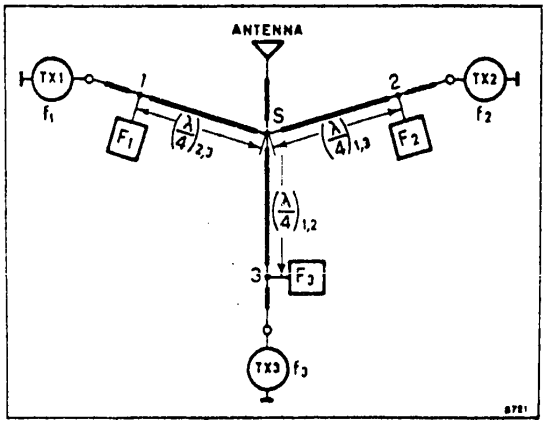

Figure 1. Diagram of FM combining unit constructed with star circuit

If one considers, for example, the TX1 transmitter with carrier at frequency f_1, the corresponding signal can transit on its own line through the F1 network but cannot reach the other two transmitters because of the strong attenuation (ideally, a short circuit) introduced at the same frequency by the F2 and F3 networks: at points 2 and 3 there is an almost total reflection that transfers, through a line section one quarter-wavelength long, the low impedance that exists at these points into high impedance at antenna-entrance point S; the TX1 therefore sees only the antenna impedance. The situation is analogous for the other two transmitters. The structure of a combiner constructed with star circuit can be different for the type of network involved, which can be of the passband type or of the blocking-filters type.

In the former type, the required characteristic is achieved with a passband filter, which can be obtained with distributed constants with two resonant elements in co-

axial cavity connected with flux linkage or capacitive coupling. Figure 2 presents one of the various solutions for constructing the passband network, obtained by means of two quarter-wave resonators and connected, with flux linkage, by means of a line of one quarter-wave electrical length; the network's response is indicated qualitatively in the same figure.

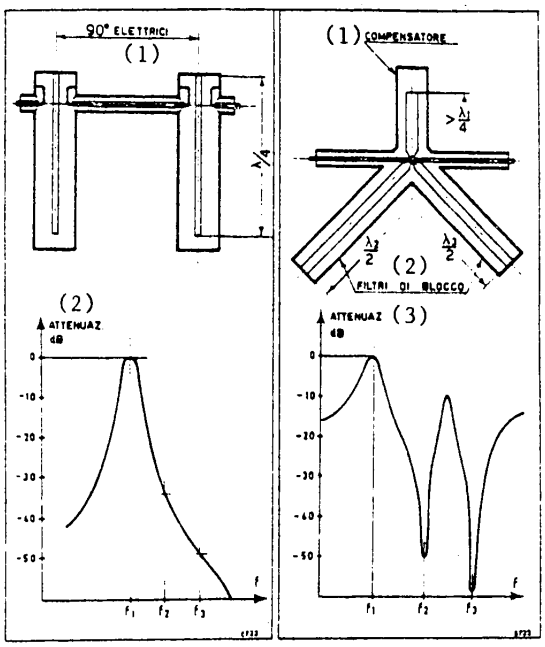

Figure 2. Filtering network of passband type and related response

Key:
1. Electric 2. Attenuation

Figure 3. Network with blocking filters and related response

Key:
1. Compensator 2. Blocking filters. 3. Attenuation

In the second type, blocking of the frequencies to be attenuated is achieved with series-resonant lines shunted off the transit line, which makes for higher isolation values, while compensation at the frequency of the carrier in transit is achieved with a line that resonates parallel with the sum of the susceptances presented by the blocking filters at the passing frequency.

Figure 3 shows a construction of the F1 network: the blocking filters are obtained with lines a half-wave long at the frequencies f_2 and f_3 and are short-circuited at their ends, while the compensator for the lowest frequency f_1 must be inductive and is achieved with a line open at the end and of length greater than a quarter-wave. The network's response in this case presents two zeros of strong attenuation at the frequencies f_2 and f_3 (Figure 3).

The figures that follow represent several examples of combining units built in the RAI Research Center, which from the beginning of FM broadcasting has been involved in the design and construction of various prototypes, different in their structure

and in the number and power of the transmitters and mass-produced, for RAI's transmitting installations, by Italian firms specializing in mechanical construction.

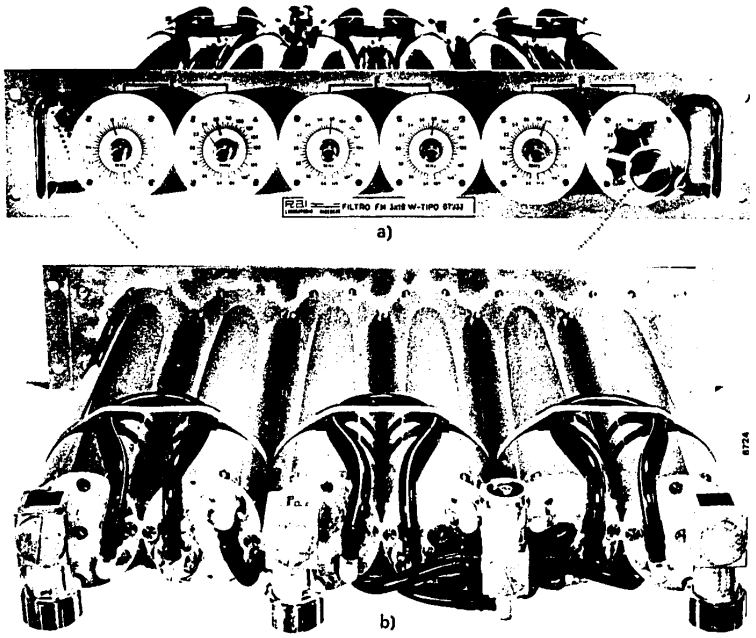

Figure 4. FM combining unit for low powers, built with star circuits. a) Front view with tuning controls; b) rear view with the cavities and the connections to the star center by coaxial cable.

Figure 4 shows the smallest specimen--as regards both power and dimensions--built for the combining of three 10-watt transmitters. It is of the star type, with passband filters each composed of two resonating cavities strongly charged capacitively so as to reduce its length and thus permit mounting it in the same section as the transmitting equipment.

Figure 5 shows a combining unit for four 3-kW transmitters; it too is of the star type with passband filters obtained with four pairs of cavities of $\lambda/4$.

The control circuits, in addition to furnishing the readings, provide for the minimum-power and maximum-reflection security, with automatic action, at the preestablished threshold, to trip off the o of the transmitters involved in the anomaly.

The quarter-wave cavities that constitute the filtering groups are of the flux-linkage type, have natural cooling, and are frequency-stabilized as regards temperature by means of a bar of Invar. They are of the type shown schematically in Figure 2.

Figure 6 shows another combining unit, for three 1-kW transmitters. This too is of the star type, but is made with blocking filters. For each of the three sections, each of which corresponds to a transmitter, the two half-wave blocking filters are

visible at the sides and the compensation lines for the channel in transit are visible at the center, per the diagram indicated in Figure 3. At the bottom of the figure are the directional probes that go to the control and security circuits.

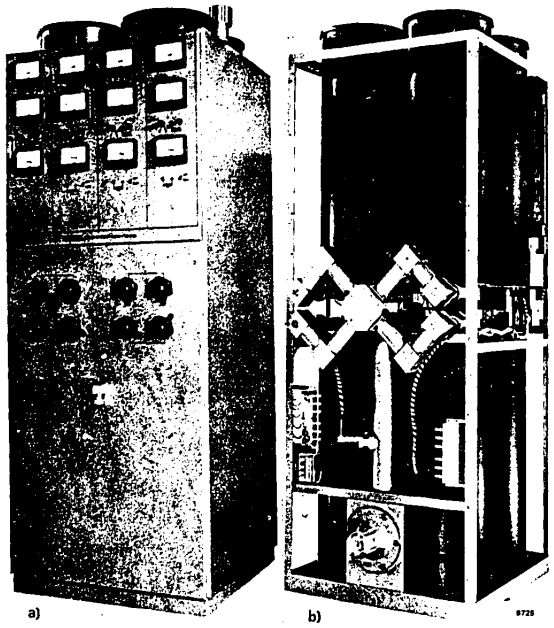

Figure 5. 4 X 3-kW FM combining unit built with star circuit. a) Front view showing the instruments for measuring power and reflection and for tuning the cavities; b) rear view showing the cavities and the star center, with the coaxial antenna line leading to it (toward the bottom).

2.2. Ring Circuit with Hybrids

When the frequencies of the transmitters to be combined are very close to one another (1.5 percent or less), star circuits are no longer suitable; in such cases it is necessary to use circuits in which the isolation between the transmitters is achieved not by the characteristic of the filtering elements but by the structure of a bridge circuit. Indeed, it is not possible to obtain high attenuation values at small percentage distances from the resonance with a parallel resonator, except at the cost of heavy losses and dangerously high gradients.

The circuits of this second group too can be differentiated by the type of filtering network (passband or band-stop) and by the type of hybrid (directional coupling at 3 dB, or a 180° hybrid--for example, a diplexer).

2.2.1. Hybrid

It will be recalled that a hybrid junction is a circuit with four gates joined two by two: the joined gates are isolated from one another. Power applied at a terminal does not appear at its conjugate but divides in equal parts between the other two

terminals; an ideal hybrid circuit is characterized by perfect adaptation of the impedances and by infinite isolation between the conjugate gates.

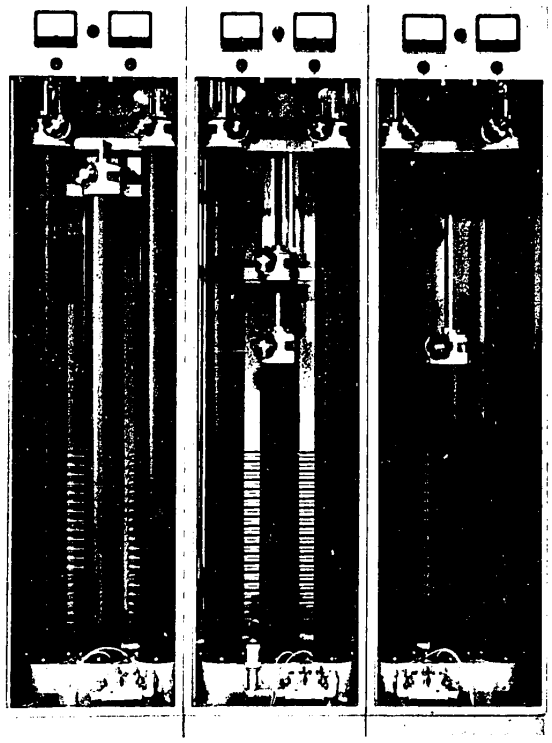

Figure 6. 3 X 1-kW FM combining unit of star type with blocking filters

In practice, a hybrid can be constructed in various forms that essentially differ as regards the phase difference between the outgoing signals, which can be 90° or 180°. The first type is constructed by coupling two parallel lines to a length of a quarter-wave (or uneven multiples) to the central frequency of its operating band; this is a 3-dB directional coupler for TEM transmission mode (Figure 7). In resonance condition (θ = 90°) and with the other gates charged on their own characteristic impedance R_c, the power applied at input gate 1 subdivides in equal parts between output gate 3 and coupled gate 4, while on conjugate gate 2 it is nil. The signal on gate 3 is delayed 90°, while that on gate 4 is in phase with the input signal:

$$E_3 = \left|\frac{E_1}{\sqrt{2}}\right| \angle 90°;\ E_4 = \left|\frac{E_1}{\sqrt{2}}\right| \angle 0°;\ E_2 = 0 \text{ (v. § 5).}$$

2.2.2. Description of Ring Circuit

The ring circuit with 3-dB hybrids and filters of passband type is described. It is composed of two hybrids and two filtering networks F identical with one another (figure 8). The power of the TX1 transmitter at frequency f_1 enters gate 1 of the first hybrid I_1, and half of it exits at gate 3 and half at gate 4; on the upper

line 3-3', the phase of the signal is 90° behind the signal going through the lower line 4-4'. The two signals can pass through the filtering networks F because they are passband filters tuned to frequency f_1; joined at gates 3' and 4' of the second hybrid, given the phase relations between the gates of that hybrid, the two signals recombine in phase at output gate 2', while they cancel one another at gate 1' because they are in counterphase on account of a futher 90° delay of the signal of the upper line. In this way, gates 1 and 1' of the circuit are isolated from one another. The second transmitter at frequency f_2 is placed at gate 1', achieving strong isolation between the transmitters independently of the characteristics of the filtering network.

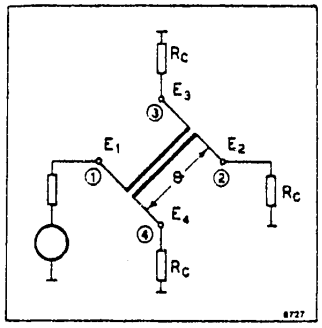

Figure 7. 3-dB directional coupler; θ = electrical length of coupling

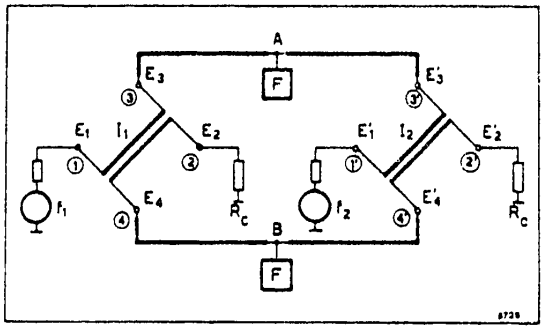

Figure 8. Diagram of FM combining unit constructed by means of ring circuit with two 3-dB couplers and two identical passband filters

The signals partially reflected by the filters F at the lateral frequencies of the f_1 transmitter travel back again behind the two lines A-3 and B-4, going back into phase at gate 2 (absorption load) of the first hybrid, not being able to return to input gate 1, where they cancel one another because they are in counterphase. This means that that circuit is at constant input impedance, being the reflection of the filters F dissipated in absorption load R_c.

The power of the TX2 transmitter at frequency f_2 applied at gate 1' of the second hybrid I_2 exits, half at gate 3' and half at gate 4', being still, in this case, the signal on the upper line, phase-delayed 90° vis-a-vis the corresponding signal of the lower line. At points A and B, these two signals undergo almost total reflec-

tion because f_2 is in the attenuated band of the filters and reenter the same hybrid, going back into phase at output gate 2', while they cancel one another, being in counterphase, at entrance gate 1' of transmitter f_2; gate 1' is also at constant input impedance.

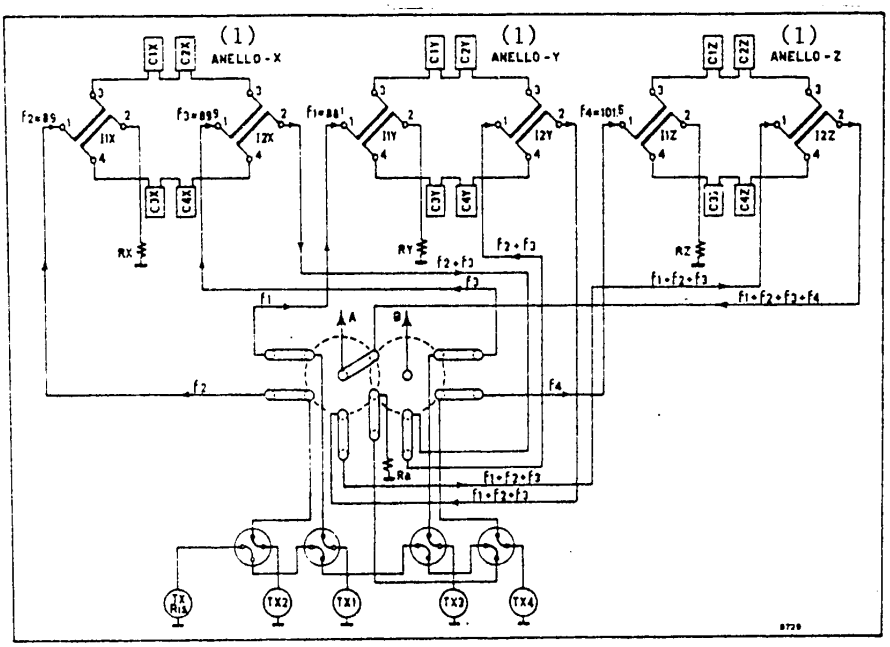

Figure 9. General diagram of 4 X 10-kW FM combining unit of Mt Venda, with switching circuits

Key:
1. Ring

Since the filters' attenuation at frequency f_2 is not infinite, a small fraction of power transits beyond the filters, reentering at gates 3 and 4 of the first hybrid and recombining in phase at gate 2 on the absorption load, while it cannot reenter at 1: this ensures isolation of the transmitters at frequency f_2 also.

One notes that while the f_1 channel is narrow-band--that is, suitable for transit of a single transmitter corresponding to the passband of the filters--the f_2 channel is wide-band, because it corresponds to the attenuated band of the filters. This makes it possible to apply to that channel two or more transmitters already combined with one another and in any case well-removed from one another in the FM band. In this way it is possible (Figure 9), with successive rings in cascade, to combine a large number of transmitters with one another (n transmitters by means of n-1 rings).

Another circuit, entirely similar, can be obtained by the use of filtering networks of dual type.

3. Mt Venda Installation

RAI, with its program to restructure a sizable part of its FM installations, set the objective of going ahead with renewal of the old equipment while at the same time making the installations suitable for stereophonic transmissions; within this framework, nearly universal introduction of circular polarization in place of horizontal polarization has been planned, in view of the considerable use advantages offered.

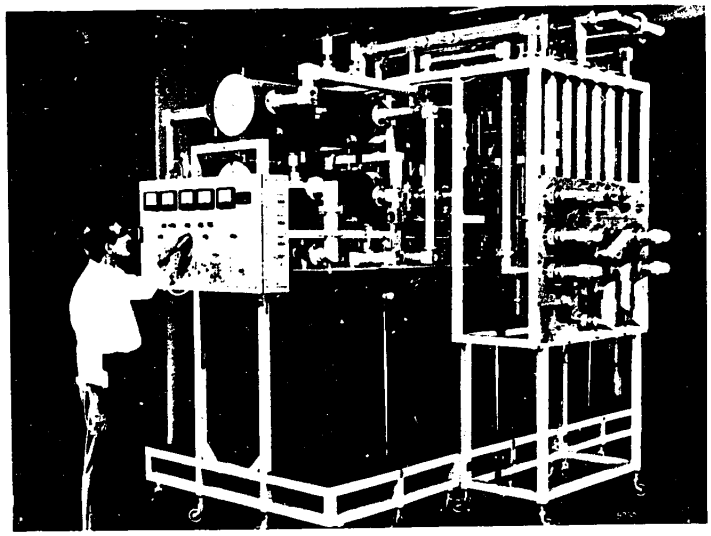

Figure 10. Overall view of the 4 X 10-kW combining unit. At left, the instrument panel; at right, the switching panel.

Within the program for renewal of the FM installations, the Mt Venda Transmitting Center presented several difficulties, occasioned essentially by the extreme closeness between the channelized frequencies, which are only 0.9 MHz apart, as against the distance of 2 MHz or more in most of RAI's FM installations.

In the old arrangement, the installation had two superimposed radiating systems, one of which radiated the combined power of the two transmitters farthest apart in frequency, while the other radiated the power of the transmitter at the central frequency; this was because of the lack, at the time, of a combining unit capable of handling three frequencies so close to one another.

At the time of the restructuring of the installation, in the transition to circular polarization it was seen to be necessary not to decrease the equivalent radiated power horizontally, which was possible only by taking up the entire space available on the metal lattice by means of a single antenna of higher gain. The problem of a combining unit suitable for simultaneous broadcasting by all the transmitters on a single antenna was posed again in this way.

The combining unit for the Mt Venda transmitting installation was built for four 10-kW FM transmitters at the frequencies of 88.1-89.0-89.9-101.5 MHz by the combining of three rings with 3-dB hybrids and passband filters of the type described; this choice was due to the very small distance between the first three frequencies.

Figure 9 is a general diagram of the combining unit, comprising the manual switching system, which is integrated with it and which in normal operating conditions has the contacts disposed as indicated in the figure. It permits both switching of the transmitters from the combining unit directly to antenna lines A and B and sectioning of the unit itself in case of breakdown, because of the fact that each of the three rings of which it is composed can function autonomously. The A (preferential) and B lines go to the two semiantennas into which the entire antenna can be sectioned in case of breakdown of a part of it. Under normal operating conditions, the two semiantennas are connected in parallel on line A.

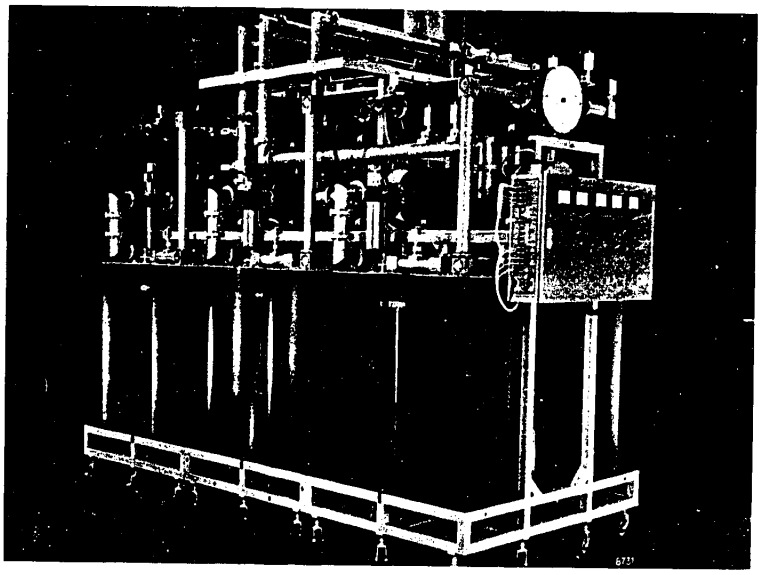

Figure 11. Rear side view of the 4 X 10-kW combining unit

Figure 10 shows a view of the unit. At left front is the control-instrument panel; on the right is the switching and sectioning frame. In the upper part the hybrids are visible, and below, the passband cavities. Figure 11 shows a rear side view.

In the following sections is described the structure of several constituent parts of a combining unit for FM transmitters, with particular attention to several design elements and with special reference to the unit built for Mt Venda.

4. Structure of the Hybrid

In section 2.2.1. there was defined a hybrid in the form of a directional coupler with a single quarter-wave section. When the power applied is high, the coupled lines in practice are normally brought back to the form of bars of rectangular or circular section, though the latter are not suitable for high coupling values.

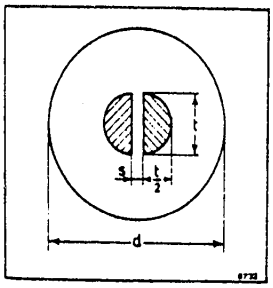

Figure 12. Cross-section of a semicircular-bar hybrid of the type used in the 4 X 10-kW unit

A less common structure is that which uses coupled lines of semicircular section placed between two parallel planes (Bibliography 3). A direct derivation of this type of structure has been used for the coupliers installed in the Mt Venda combining unit (Figure 12). The advantages of this configuration were seen to lie in the large coupling area, together with reduced cross-section. For a coupler of quarter-wave section and characteristic impedance of 50 ohms, the dimensional ratios of the section indicated in Figure 12 prove to be: t/d = 0.3449 and s/d = 0.05342.

5. Relation between the Voltages of a Hybrid and of a Ring of Hybrids

5.1. Voltages at the Outputs of a 3-dB Coupler

A coupler is considered that is composed of two parallel transmission lines coupled uniformly for an electrical length θ, with power supplied at gate 1 and closed at the other gates on characteristic impedance R_c (Figure 7).

It is demonstrated (Bibliography 1, 2) that the voltages at the other gates are:

[1] $$E_3 = E_1 \frac{\sqrt{1-k^2}}{\sqrt{1-k^2}\cdot\cos\vartheta + j\sin\vartheta}$$

(output gate)

[2] $$E_4 = E_1 \frac{jk\sin\vartheta}{\sqrt{1-k^2}\cdot\cos\vartheta + j\sin\vartheta}$$

(coupled gate)

in which k is the coupling factor that corresponds to the maximum value of the ratio E_4/E_1 for $\theta = 90°$ (centerband of the hybrid).

From [1] and [2] it results that for any value of θ--that is, with the variation of the frequency of the input signal--$|E_3|^2 + |E_4|^2 = |E_1|^2$; that is, all the input power is collected at gates 3 and 4, and therefore at the conjugate gate $E_2 = 0$. In addition, the input impedance is constant and equal to R_c at all frequencies.

In the particular case of a 3-dB coupler that has to be $E_3 = E_4$ for $\theta = 90°$, it results from [1] and [2] that $k = 1/\sqrt{2}$. Therefore, for the 3-dB coupler the preceding relations become:

[3] $$E_3 = -j\frac{E_1}{\sqrt{2}}a \qquad \text{with}$$

$$a = \frac{1}{\sin\vartheta - j\frac{1}{\sqrt{2}}\cos\vartheta}$$

(output gate)

[4] $$E_4 = \frac{E_1}{\sqrt{2}}b \qquad \text{with} \qquad b = \frac{\sin\vartheta}{\sin\vartheta - j\frac{1}{\sqrt{2}}\cos\vartheta}$$

(coupled gate)

a and b are two complex operators that have the same phase angle and that can be represented with two parallel vectors whose ratio b/a = sin θ. It follows that with variation of frequency, E_3 and E_4, even though rotating phase, always remain in quadrature with one another. At the central frequency $f_o(\theta = 90°)$, a = b = 1. This type of coupler can be used in a frequency octave (between $f_o/\sqrt{2}$ and $f_o\sqrt{2}$) with a rather limited variation of the coupling, as results from [3] and [4].

5.2. Voltages at the Gates of a Ring of Hybrids

A ring is considered that is composed of two 3-dB couplers, I_1 and I_2, with two filters placed at points A and B of the connection lines (Figure 8). Analysis of the ring alone is done, for the sake of simplicity, by supposing that the filters have an ideal transfer function with the value of one at passing frequency f_1, and zero at attenuated frequency f_2--that is, as if the filters did not exist at frequency f_1 and presented a short circuit at frequency f_2. The ring's behavior is examined separately at the two frequencies.

5.2.1. Signal in Transit at Frequency f_1

When gates 1' and 2' of the second hybrid are charged with impedance R_c, input gates 3' and 4' present a constant impedance equal to R_c at all the operating frequencies. Therefore the voltages E_3 and E_4 at the output gates of the first hybrid are still the same as expressed by [3] and [4] and are also equal to the voltages at the input gates of the second hybrid E'_3 and E'_4 except for a phase constant that can be expressed by the operator

$$c = e^{-j\beta l} \quad (E'_3 = E_3 e^{-j\beta l};\ E'_4 = E_4 e^{-j\beta l})$$

which hereinafter, for simplicity of written expression, will be understood (l is the length of lines 3 - 3' and 4 - 4').

We now obtain the expressions of the voltages E'_2 and E'_1 at the output gates of the second hybrid to which are applied the voltages $E'_3 = E_3$ and $E'_4 = E_4$, respectively, at input gates 3' and 4' (Figure 13). Considering this configuration as the superimposition of two situations analogous to that indicated in Figure 7, expressions analogous to [3] and [4], respectively, are applied individually to the input gates for the corresponding output gate and coupled gate, and adding together, at the outputs, the contributions of the two input signals, one has:

[5] $$E'_2 = \frac{1}{\sqrt{2}}(bE_3 - jaE_4) = -jE_1 a \cdot b$$

$$E'_1 = \frac{1}{\sqrt{2}}(bE_4 - jaE_3) = -\frac{E_1}{2}(a^2 - b^2).$$

It is recognized immediately that if $\theta = 90°$ at frequency f_1, with a = b = 1 the signal is collected entirely at gate 2', because in such case $E'_1 = 0$; and this is because the two signals at gate 1' are in counterphase. For $\theta \neq 90°$, $E'_1 \neq 0$. and therefore a fraction of signal reaches gate 1' also, thus decreasing the isolation between the two generators at frequency f_1.

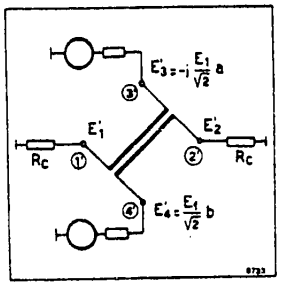

Figure 13. Voltages at the gates of the second hybrid

On the basis of [3], [4] and [5], the moduli of the voltages at the various points of the ring at frequency f_1 are:

$$[6]\quad \begin{cases} \left|\dfrac{E_3}{E_1}\right| = \dfrac{1}{\sqrt{2}}|a| = \dfrac{1}{\sqrt{2}}\dfrac{1}{\sqrt{1-\frac{1}{2}\cos^2\vartheta}} \\ \left|\dfrac{E_4}{E_1}\right| = \dfrac{1}{\sqrt{2}}|b| = \dfrac{1}{\sqrt{2}}\dfrac{\sin\vartheta}{\sqrt{1-\frac{1}{2}\cos^2\vartheta}}; \end{cases}$$

$$[7]\quad \begin{cases} \left|\dfrac{E'_2}{E_1}\right| = |a\cdot b| = \dfrac{\sin\vartheta}{1-\frac{1}{2}\cos^2\vartheta} \\ \left|\dfrac{E'_1}{E_1}\right| = \dfrac{1}{2}|a^2-b^2| = \dfrac{1}{2}\cdot\dfrac{\cos^2\vartheta}{1-\frac{1}{2}\cos^2\vartheta}. \end{cases}$$

Attention is drawn to the fact that the isolation $|E'_1/E_1|$ between the two transmitters at frequency f_1 is entrusted exclusively to the equilibrium of the ring and that its value under balancing conditions is theoretically infinite at the hybrid's resonance frequency ($\theta = 90°$; a = b = 1) in relation to the vectorial combination, at gate 1', of two magnitudes of equal amplitude and in counterphase. This requires that in addition to having perfect symmetry in the mechancial structure of the two branches of the ring, the two filters be identical and remain so in time: a small variation in the tuning of one filter vis-a-vis the other, because of mechanical or temperature factors, can cause a considerable loss of isolation (as can be verified with the second of the expressions of [5] by multiplying E_3 and E_4 by the characteristic of the filters). This requires the use of cavities that are very stable in frequency.

5.2.2. Signal Reflected at Frequency f_2

Analysis of the f_2 signal is identical in form to analysis of the f_1 signal.

A circuit section downstream from points A and B (Figure 8) is considered, keeping in mind the description given, in section 2.2.2., in relation to the TX2. If, initially, one ignores the wave that travels on the two lines toward points A and B and one supposes that the wave reflected at those points is, instead, a traveling wave coming from two imaginary generators at A and B, the conditions already examined at frequency f_1 are found again: the signal on the upper line phase-delays 90° vis-a-vis the corresponding signal of the lower line, and the situation is still represented by Figure 13, the generators having in this case the amplitudes:

$$E'_{3R} = -j\frac{E'_1}{\sqrt{2}}a|\rho|e^{j(\psi-2\beta s)}$$

$$E'_{4R} = \frac{E'_1}{\sqrt{2}}b|\rho|e^{j(\psi-2\beta s)} \qquad [8]$$

in which the subscript R is introduced to recall that two signals reflected at frequency f_2 are involved. In addition, there is E'_1 instead of E_1, in conformity with the amplitudes at the gates of the respective generators; $|\rho|$ and ψ are the modulus and the phase of the coefficient of reflection of the filtering networks at points A and B, and s is the distance between the latter and the hybrids.

In the case hypothesized for the transfer function: $|\rho| = 1$; $\psi = \pi$, and except for a phase constant which, not being essential, is understood, the expressions of [8] are identical in form to the expressions indicated in Figure 13, corresponding to [3] and [4]. In practice, $|\rho|$ is very close to unity, and therefore the simplifying hypothesis does not alter the conclusions.

With this premised, the signals at frequency f_2--E'_{2R}/E'_1 and E'_{1R}/E'_1, exiting at gates 2' and 1', respectively--are expressible by means of the same expressions as in [5] and [7], in which, in this case, θ is calculated at f_2. One notes that when the ratio E'_1/E_1 is calculated at f_1, it represents the isolation of the ring between the two generators at f_1, and when it is calculated at f_2, it represents the coefficient of reflection at gate 1'.

In Figure 14, the magnitudes examined in function of the electrical length θ of the coupler and of normalized frequency f/f_o ($f/f_o = \theta/90°$) are represented in dB.

The first graph indicates, in accordance with [6], the course of the voltages at the output and coupled gates of the first hybrid with voltage applied at gate 1. The second graph represents the ring's output at gate 2' both for the signal at f_1 and for the signal at f_2, in accordance with the first expression of [7]. The third graph represents both the isolation of the ring at F_1 and the return losses at gate 1' at frequency f_2 on the basis of the second expression of [7].

6. Filtering Networks

6.1. Considerations on the Transfer Function of the Filter

Analyzing the requirements for the filtering networks, one easily recognizes the factors that introduce losses and distortions.

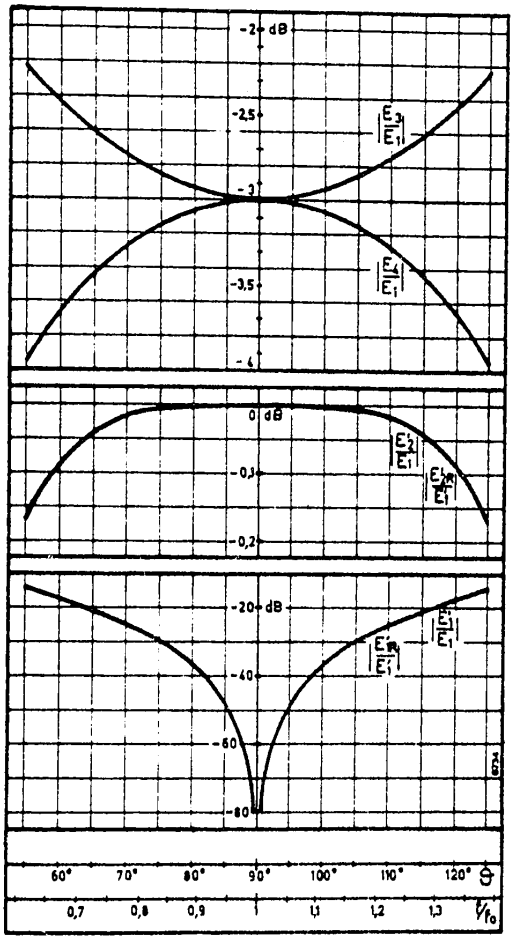

Figure 14. Top: course of the voltages at the output gate and at the coupled gate of the first hybrid in relation to the input voltage. Middle: course of voltage at the output gate of the second hybrid in relation to the input signal at the two different frequencies. Bottom: isolation at frequency f_1 and return losses at frequency f_2.

Passing channel 1, encountering an amplitude characteristic that is not perfectly flat and a phase characteristic not perfectly linear, undergoes an alteration in the amplitude and the phase of the spectral spectral lines that constitute the modulated signal entering, with consequent distortions and power loss in the outgoing signal: a loss from dissipation at the center of the channel, and predominantly by reflection at the extremes.

Reflected channel 2 encounters the characteristic at one side at frequency f_2. Keeping it in mind that the useful signal, in this case, is the reflected one, and that the characteristic does not present an infinite attenuation value, part of the signal passes and dissipates on the absorption charge with loss of power, while the

useful signal undergoes a dissymmetrical treatment of the side bands, being reflected on a side of the characteristic that presents an attenuation and therefore a coefficient of reflection variable with the frequency within the framework of the channel; and this gives rise to distortions.

The designing of the filtering network can therefore be premised on study of the transfer function H of the passband at the frequencies of channel 1 and of transfer function H_R for reflected channel 2, which in this case is represented by coefficient of reflection ρ at the input of the same network at the frequencies of channel 2--a coefficient that must prove close to unity and variable very little within the framework of the channel.

6.1.1. Width of the FM Channel

The band width necessary for transmission of the FM channel is conventionally assumed to be $\pm$ 100 kHz; but in contrast to the television channel, a radiofrequency tolerance mask is not required. What is required under the heading of technical specifications, though, is all the characteristics and tolerances for the demodulated signal in both multiplex and monophonic operation (amplitude-frequency characteristic, nonlinear distortion, AM synchronous modulation, linear and nonlinear diaphony between the A and B channels).

This fact allows a certain freedom in case-by-case definition of the band characteristics, permitting simplifications with reduced losses and distortions in the case of adjacent channels farther away from one another; but it requires careful study of the transfer function of the filters in the opposite case.

The band width necessary can be calculated with the well-known approximate expression called Carson's rule; but more rigorously, it is possible to put the channel width into relation with the percentage of power transmitted by it, referring to [38] and [41] in the Appendix, by means of which Table 1 was calculated.

6.2. Elementary Component of the Filter

The filter is constructed on a distributed-constants basis with passband elements. The simplest element of this type would be composed of a line of length s equal to a quarter-wave at frequency f_1 and circuited at the extremity, shunted off the transmission line (Figure 15a), which, as is known, behaves, around the first resonance, like a parallel resonant circuit. (The representation as a two-wire line is by way of example.)

In Figure 15b is shown the equivalent circuit with the values of the elements L, C, R_p expressed in function of the characteristics of the distributed-constants resonator (see Table 1, Bibliography 6); l, c, α are, respectively, the inductance, the capacity and the constant of attenuation per unit of length.

It should be said at once that an element of this type is not suitable for solving the problem under consideration. Indeed, the filter's characteristic must go from negligible attenuation values at frequency f_1 to quite high values at frequency f_2 in a percentage interval of frequency $\Delta f/f$ of about 1.1 percent. This requires a variation of the input admittance Y_e of the element, in the vicinity of the very high f_1 resonance; Y_e can be represented (within the limits of validity expressed in Table 1, Bibliography 6) with the expression:

Table 1

$\delta f = \pm 75$ kHz

Modulating frequencies (kHz)	Channel Width ~ ±100 kHz: Channel used (kHz)	Power Fraction Transmitted	Fraction of Total Power Q ≥ 99.99%: Channel used (kHz)	Power Fraction Transmitted
1			± 82	0.99990
5			± 100	0.99998
10	± 100	0.99948	± 110	0.99994
15	± 105	0.99926	± 120	0.99993
10 + 15*	± 105	0.99978	± 120	0.99999
Stereo**	± 106	0.99564	± 159	0.99991

* Two tones of half-amplitude in relation to the single tone, which varies by ± 75 kHz.

** Lines f_1 = 23 kHz and f_2 = 53 kHz, obtained by modulating the right and left channels with two tones in counterphase of frequency f_m = 15 kHz, each of one-half amplitude.

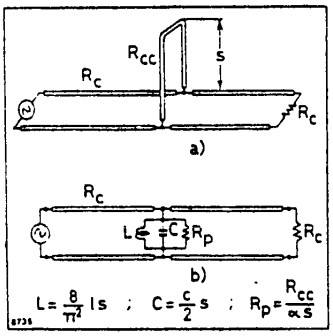

Figure 15. a) distributed-constants resonator shunted off transmission line of characteristic impedance R_c; b) equivalent circuit in vicinity of first resonance. l, c, α are the inductance, capacity, and attenuation constant per unit of length of the distributed-constants resonator.

[9] $$Y_e \cong \frac{\pi}{4}\frac{1}{Q \cdot R_{cc}} + j\frac{\pi}{2}\frac{1}{R_{cc}}\frac{\Delta f}{f_1}$$

with $\Delta f = f - f_1$; R_{cc}, characteristic impedance; and Q, coefficient of quality of the resonator. In other words, Q being practically constant in the vicinity of Δf, the derivative $|dY_e/df| = \pi/2f_1R_{cc}$ has to be large and therefore the characteristic impedance R_{cc} has to be small. The order of magnitude of R_{cc} can be deduced from a practical case relative to the X ring of the Mt Venda unit (f_1 = 89 MHz; f_2 = 89.9 MHz). With a value of $|\rho| \cong 0.99$ placed on f_2, $R_{cc} \cong 0.13$ ohm would result (see also [22]). The practical impossibility of physically achieving such low values of the characteristic impedance of line s is obvious.

It is nevertheless possible to reduce the characteristic impedance of a parallel resonant circuit by coupling the resonator to the external circuit in such a way as to reduce the impedance level to the value desired. This is possible by means of devices of a magnetic or electrical nature. The former case can in theory be achieved by means of an impedance transformer.

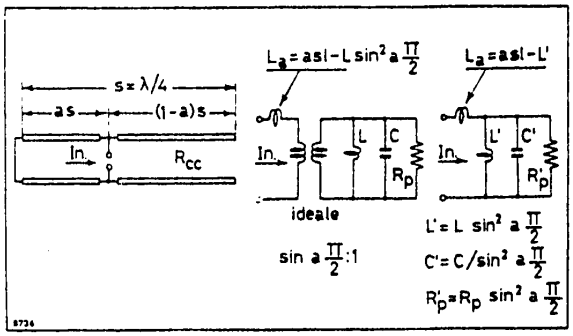

Figure 16. Transformation of characteristic impedance by means of a parallel distributed-constants resonant circuit; equivalent circuits L, C, R_p have the same values as indicated in the preceding figure.

Figure 16 shows a simple transformation method capable of reducing the degree of (a < 1) coupling of the resonator to the line to which it is connected.

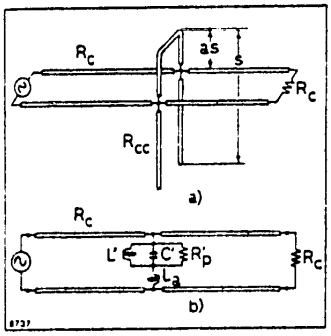

Figure 17. a) distributed-constants resonator with intermediate input connected to the transmission line; b) equivalent circuit.

The equivalent circuit, valid in the vicinity of the first resonance ($s = \lambda_1/4$) and indicated in the same figure, shows the same values L, C, R_p valid for the quarter-wave resonator when it is connected at its open end to the transmission line, and takes into account the change of impedance with an ideal transformer that has a sin ratio $\sin(a/2):1$, which is the ratio between the voltage at the intermediate input and the voltage at the open end. The new configuration is represented in Figure 17 together with its equivalent circuit.

One notes important differences from the preceding case:

1) The level of the impedances is lower; in fact, the impedance of each element is $\sin^2(a\pi/2)$ times the corresponding impedance for connection to the open terminal. In addition, while on the one hand the level of characteristic impedance from the value R_{cc} to the value $R'_{cc} = R_{cc} \sin^2(a\pi/2)$ goes down, as is desired, this entails, at equal Q, an increase in the losses, with the resistance R_p, which represents the equivalent of the losses in the resonator, dropping in the same ratio.

2) The voltage at the open end increases in the ratio $1/\sin(a/2)$ vis-a-vis the input voltage, and with it, all the electrical stresses in the resonator, including the reactive power.

3) The coupling to an autotransformer introduces a coupling reactance $\omega \cdot L_a$, in which $L_a = asl - L \sin^2(a\pi/2)$ that cannot always be ignored.

The effect of the coupling reactance is to introduce several modifications into the course of the transfer function, with regard to the L'C' circuit only. Indeed, this last-named circuit resonates parallel to frequency f_1 and is capacitive at frequencies higher than f_1. Consequently there exists a frequency $f_s > f_1$ at which that element is in series resonance with L_a, and the resonator's curve of reactance therefore contains a pole at frequency f_1 and a zero at a higher frequency f_s. The zero gets closer to the pole, on the axis of the ω's, as the coupling reactance increases with respect to resonance reactance $\omega_1 L'$, or the higher the transformation ratio is; at the same time, the asymmetry of the characteristic increases with respect to central frequency f_1, and therefore the attenuation of the circuit for a given distance Δf from f_1 vis-a-vis the attenuation at $-\Delta f$.

In the distributed-constants circuit, the parallel resonance is determined by the entire length $s = \lambda_1/4$ of the resonator, and the series resonance by the line section $(1 - a)s$ open at the end when, at frequency f_s, it becomes in turn a quarter-wave long.

The value of the admittance at the resonator input in the vicinity of the resonance can be represented by the approximate expression:

[10] $$Y = \frac{\pi}{4QR_{cc}\sin^2\left(a\frac{\pi}{2}\right)}\left[1 + j\,2Q\,\frac{\Delta f}{f_0}\right]$$

(see Table 1, Bibliography 6) in which $\Delta f = f - f_o$, with f_o with f_o = resonance frequency, Q = coefficient of quality of the coaxial line charged with the losses intrinsic to the resonator only (see section 8), and R_{cc} = characteristic impedance of the resonator. It is valid in the vicinity of the first resonance under the conditions $|\Delta f/f_o| \ll 1$ and

[11] $$\left| \frac{\Delta f}{f_0} \frac{\frac{\pi}{2}}{\operatorname{tg}\left(a\frac{\pi}{2}\right)} \right| \ll 1.$$

[10] was obtained by means of series developments applied to the equations of the lines with losses, and condition [11] results from the first term that was ignored in the development.

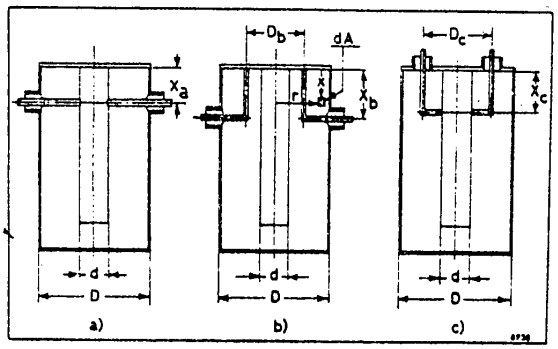

Figure 18. Equivalent structures with autotransformer and transformer. a) direct coupling; b), c) turn-of-winding coupling.

The autotransformer structure so far considered (Figure 18a) is in practice used for high degrees of coupling. In addition, it represents an easy term of transition, by means of equivalence systems, in the calculation of transformer structures with turn-of-winding coupling (Figure 18b, c); these latter are prefereable for high transformation ratios. The procedure consists in determining the dimensions of the turn that produce the same concatenated flux as the autotransformer. In the case of Figure 18b), for example, by making the flux of the turn-of-winding equal to that relative to the autotransformer ofFigure 18a), one obtains the equivalence condition:

[12] $$\sin \beta X_b \cdot \log D/D_b = \sin \beta X_a \cdot \log D/d \quad \text{[turn-of-winding b]}$$

in which $\beta = 2\pi/$ and the other magnitudes are indicated in Figure 18.

Analogously, in the case of Figure 18c) one obtains:

[13] $$\sin \beta X_c \cdot \log D_c/d = \sin \beta X_a \cdot \log D/d \quad \text{[turn-of-winding c]}$$

The turn-of-winding resonator thus obtained retains, in the vicinity of the resonance, the same characteristics as the autotransformer resonator--in particular, the same ratio of transformation and the same electrical stresses--except for the value of the coupling reactance, which, in order to be in relation with the inductance of the turn-of-winding, can take on different values. The input admittance of the turn-of-winding coupled resonator is still represented by equation [10].

6.3. Filtering Network of the Combining Unit

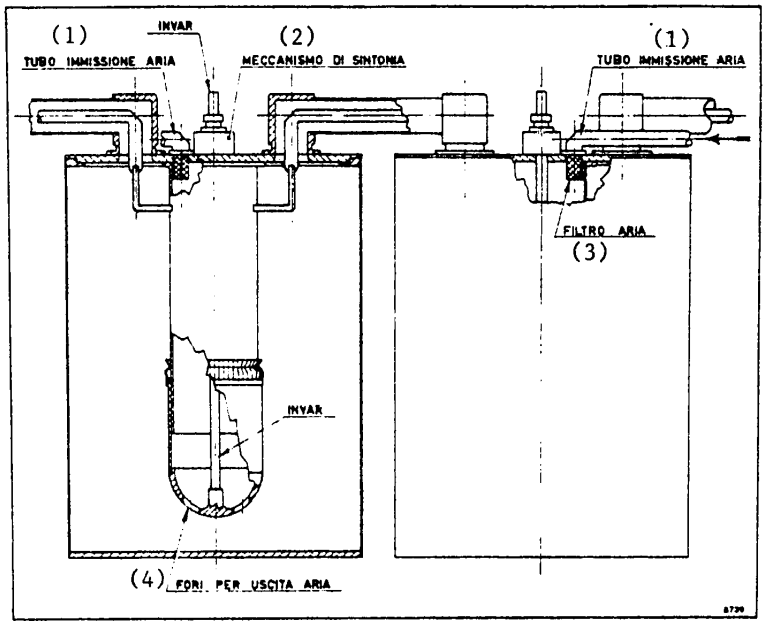

Figure 19. Cavities of passband type coupled inductively for the Mt Venda filter

Key:
1. Air-inlet tube
2. Tuning mechanism
3. Air filter
4. Holes for air outlet

The selectivity characteristics necessary for the networks of the combining unit for Mt Venda are obtained by means of two identical elements of the type described, turn-of-winding coupled by means of a quarter-wave line (Figure 19). The equivalent circuit of the filter thus obtained is represented in Figure 20: it expresses a passband characteristic; its transfer function in the vicinity of the resonance ($|\Delta f/f_o| \ll 1$), with the limitations considered, is expressed in modulus and phase by

[14] $$|H_2| = \frac{2r^2}{\{[4(r+1)Q\,\Delta f/f_0]^2+[r^2+(r+1)^2-(2Q\,\Delta f/f_0)^2]^2\}^{1/2}}$$

[15] $$\Phi_2 = \operatorname{artg}\frac{(2Q\,\Delta f/f_0)^2 - r^2 - (r+1)^2}{4(r+1)Q\,\Delta f/f_0}$$

in which the normalized impedance values $r = R/R_c$ and $x = X/R_c$ are, for [10]

[16] $$r = \frac{R_{cc}}{R_c}\,\frac{4}{\pi}\,Q\,\sin^2(a\pi/2),$$

[17] $$x = \frac{R_{cc}}{R_c}\,\frac{2}{}\,\frac{\sin^2(a\pi/2)}{\Delta f/f_o}$$

from which there results:

[18] $$\frac{r}{x} = 2Q\ \Delta f/f_o\ ;$$

a circuit of this type therefore proves to be completely defined by three parameters, thus chosen: f_o, Q, r.

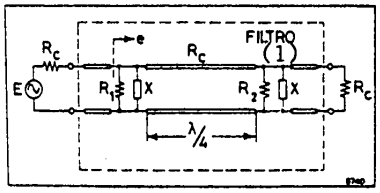

Figure 20. Equivalent circuit for filter obtained with two identical cavities coupled with quarter-wave line.

Key:
1. Filter

Figure 21 illustrates the characteristics of the system adopted. In the upper part of the figure is drawn the curve A_2 of insertion attenuation derived from [14]:

[19] $$A_2 = 10\ \log_{10}\frac{1}{|H^2|^2}[dB]$$

with the values stabilized for ring X: f_o = 89 MHz; Q = 14,650; r = 51. The other magnitudes that appear in the preceding expressions are (still for ring X): characteristic impedance of circuit R_c = 50 ohms; characteristic impedance of the cavities R_{cc} = 76.77 ohms; degree of coupling a = $2.69 \cdot 10^{-2}$, and therefore, transformation ratio 1/sin (a π/2) = 23.7 In the same figure, insertion attenuation A_2 of a single cavity is shown in a broken line, together with the values measured.

In the lower part of Figure 21 are drawn the phase curves and the group delay.

One notes several characteristic values of the curves relative to ring X:

Attenuation at carrier f_1	- 0.17 dB
Attenuation at ± 100 kHz	- 0.38 dB
Attenuation at carrier f_2	- 24.57 dB
Band width at -3 dB	520 kHz
Group delay in channel ± 100 kHz	151 ns

6.4. Coefficient of Reflection

It has already been noted (section 6.1.) that coefficient of reflection ρ at the input of the filtering network represents the transfer function H_r for the reflected channel when it is calculated in the band of channel 2. In addition, if calculated at the frequencies of channel 1 it furnishes the value of the power lost through reflection by transmitter 1 in transit and dissipated in the absorption load.

Calculation of requires knowledge of the input impedance at section e of the filtering network (Figure 20). With simple calculations it is possible to transform

all the elements of the network at section e into the two elements in parallel R_e and X_e (Figure 22). Impedance Z_e at the filter input is then:

[20] $$\frac{1}{Z_e} = \frac{1}{R_e} + \frac{1}{jX_e}$$

in which the active and reactive components normalized at impedance R_c are:

[21] $$\frac{1}{r_e} = \frac{1}{r} + \frac{1 + 1/r}{(1 + 1/r)^2 + (1/x)^2},$$
$$\frac{1}{x_e} = \frac{1}{x} - \frac{1/x}{(1 + 1/r)^2 + (1/x)^2}.$$

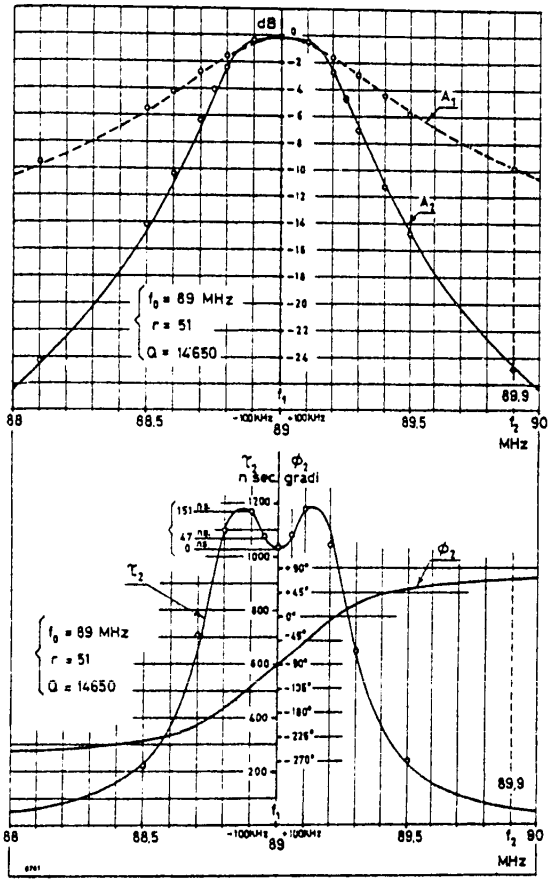

Figure 21. Top: course of insertion attenuation for two-cavity filter (curve A_2) and one-cavity filter (curve A_1); bottom: course of phase and group delay for the two-cavity filter. The small circles indicate the values measured.

Key:
1. Degrees

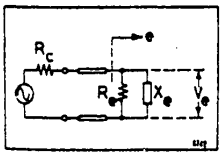

Figure 22. Transformation at network-elements input indicated in Figure 20.

The modulus and the phase of the coefficient of reflection at input $\rho = Z_e - R_c / Z_e + R_c$ are as:

[22] $$|\rho| = \left[1 - \frac{1}{\frac{1}{2} + \frac{1}{4}(r_e + 1/r_e) + r_e/(4x_e^2)}\right]^{1/2}$$

[23] $$\psi = \operatorname{artg} \frac{2/x_e}{1 - 1/r_e^2 - 1/x_e^2}.$$

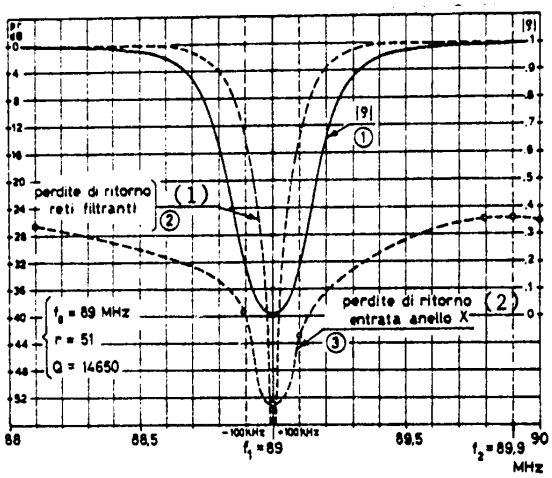

f		Coefficente di riflex. |9| (3) reti filtranti	Perdite di ritorno p.r. = 10 log 1/|9|² (1) reti filtranti
TX_2	- 100 kHz	0,9956	
	- 50 "	0,9964	
	f_2 = 89,9 MHz	0,9970	
	+ 50 kHz	0,9975	
	+ 100 "	0,9979	
TX_1	- 100 kHz		14,00 dB
	- 50 "		25,83 "
	f_1 = 89 MHz		74,69 "
	+ 50 kHz		25,83 "
	+ 100 "		14,00 "

Figure 23. Modulus of coefficient of reflection ρ (curve 1); return losses at filter input (curve 2); return losses at ring input (curve 3)

Key:
1. Return losses, filtering networks
2. Return losses, ring-X input
3. Coefficient of reflection, filtering networks

The course of the modulus $|\rho|$ at the network input as expressed by [22] is drawn in Figure 23 (curve 1) for the values of f_o, r and Q achieved for ring X. The values for the channel of the TX2 are given in the table that accompanies Figure 23.

In the same figure, graph 2 relative to the network's return losses is drawn, and these losses are presented in a table for channel 1. Finally, in curve 3 are given, for comparison with curve 2, the return losses measured at the ring-X input. For transit channel 1, these losses are higher than 40 dB; this means, as already noted, that the reflection of the networks is almost entirely sent into the absorption load.

Still for ring X, the group delay in channel 2 was calculated by using [23]:

[24] $$\tau R = \frac{1}{2\pi} \frac{d\psi}{df}$$

and proved to be 30.8 ns within the framework of the channel's $\pm$ 100 kHz as against the 151 ns relative to transit channel 1.

Before concluding on this subject, it is noted that the quarter-wave line that couples the cavities (Figure 20) was considered to be of constant electrical length with variation of frequency. It is pointed out that all the formulas were derived also without introducing this approximation, and it was verified that at least in the field of frequencies considered, the errors introduced with this simplification prove lower than 0.5 percent for all the magnitudes calculated, while the formulas not simplified are formally somewhat more complex; and therefore this approximation was accepted.

7. Distribution of the Powers of the Transmitters in the Elements of the Unit

With the losses in the connection lines and in the hybrids considered as negligible (the values measured are on the order of hundredths of a dB), the power drawn by two transmitters of a ring is distributed into six elements (Figure 24). The part P_{RC} reaches the useful load R_c that can be the antenna or a following ring; a second part P_{RL} dissipates on the absorption load; and the other four parts, $2P_{R1}$ and $2P_{R2}$, are absorbed by the four cavities and dissipated in the elements diagrammed with the equivalent resistances at losses R_1 and R_2 in Figure 20.

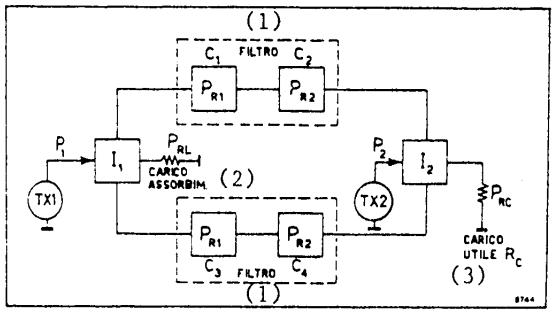

Figure 24. Distribution of the input powers in the elements of the ring

Key:
1. Filter 2. Absorption load 3. Useful load

It is useful to know the distribution of the power of the transmitters, both for evaluating the losses and for the dimensioning and disposal of the dissipated heat.

7.1. Nonmodulated Transmitters

A single branch of the ring is initially considered: it is presumed to apply power to the two-cavity filter examined (Figure 20) with a sinusoidal generator of available power P_1. Part of the incident power $P^+ = P_1$ is reflected by the filter because at the input (section e), the coefficient of reflection is different from zero. The reflected power $P^- = |\rho|^2 P_1$ constitutes the return loss expressed in watts. The part of power P_e that effectively enters the filter is the difference of the preceding ones: $P_e = (1 - |\rho|^2)P_1$. This is distributed in the elements R_c (useful load), R_1 and R_2 (cavities). The active power $P_e = |V_e|^2/R_e$ (Figure 22) dissipated in the imaginary resistance R_e is in reality dissipated in the resistive elements of the filter per a distribution that can be derived from analysis of the network (Figure 20) and that is:

[25] $$P_{RC} = P_e \cdot \alpha, \quad P_{R1} = P_e \cdot \beta, \quad P_{R2} = P_e \cdot \gamma,$$

in which the quantities α, β, γ indicate the fractions of power P_e dissipated, respectively, in R_c, R_1 and R_2; their values are expressed by:

[26] $$\alpha = \frac{r}{(1+r) + (1+1/r)^2 + (1/x)^2},$$

$$\beta = \frac{\left(1+\frac{1}{r}\right)^2 + \left(\frac{1}{x}\right)^2}{(1+r) + (1+1/r)^2 + (1/x)^2},$$

$$\gamma = \frac{1}{(1+r) + (1+1/r)^2 + (1/x)^2},$$

in which r and x are again furnished by [16] and [17]; one has $\alpha + \beta + \gamma = 1$.

The extension of these considerations to the complete ring (Figure 24) is immediate.

For transmitter 1, one has:

[27] $$\begin{cases} \frac{P_{RC}}{P_1} = (1 - |\rho|^2) \cdot \alpha, \\ \frac{P_{R1}}{P_1} = \frac{1}{2}(1 - |\rho|^2) \cdot \beta, \\ \frac{P_{R2}}{P_1} = \frac{1}{2}(1 - |\rho|^2) \cdot \gamma, \\ \frac{P_{RL}}{P_1} = |\rho|^2, \end{cases}$$

in which, if the values of $|\rho|$ and of the parameters α, β, γ are calculated at carrier frequency f_1, the expressions of [27] express the power distribution of nonmodulated transmitter 1.

Analogously for transmitter 2:

[28]
$$\begin{cases} \frac{P_{RC}}{P_2} = |\rho|^2, \\ \frac{P_{R1}}{P_2} = \frac{1}{2}(1-|\rho|^2)\cdot\gamma, \\ \frac{P_{R2}}{P_2} = \frac{1}{2}(1-|\rho|^2)\cdot\beta, \\ \frac{P_{RL}}{P_2} = (1-|\rho|^2)\cdot\alpha \end{cases}$$

with $|\rho|$, α, β, γ calculated at carrier frequency f_2 of transmitter 2.

The factors 1/2 that appear in the preceding formulas take account of the subdivision of power of each transmitter on the two branches of the ring.

7.2. Modulated Transmitters

When the transmitters are modulated, the power distribution varies. With a non-modulated carrier, all the power of a transmitter is associated with the carrier; with a modulated carrier, in accordance with Parseval's equation, the power associated with the modulated signal is the sum of the powers carried by the individual lines of the spectrum. Referring to Appendix A, formulas [37] and [38], and modulating with a sinusoidal tone of frequency f_m, the expressions of [27] relative to transmitter 1 modify into the following:

[29]
$$\begin{aligned} \frac{P_{RC}}{P_1} &= [(1-|\rho_k|^2)\cdot\alpha_k\cdot J_k^2(m)]_{k=0} + \\ &\quad + 2\sum_{k=1}^{n}(1-|\rho_k|^2\cdot J_k^2(m), \\ \frac{P_{R1}}{P_1} &= \frac{1}{2}[(1-|\rho_k|^2)\cdot\beta_k\cdot J_k^2(m)]_{k=0} + \\ &\quad + \sum_{k=1}^{n}(1-|\rho_k|^2)\cdot\beta_k\cdot J_k^2(m), \\ \frac{P_{R2}}{P_1} &= \frac{1}{2}[(1-|\rho_k|^2\cdot\gamma_k J_k^2(m)]_{k=0} + \\ &\quad + \sum_{k=1}^{n}(1-|\rho_k|^2)\cdot\gamma_k\cdot J_k^2(m), \\ \frac{P_{RL}}{P_1} &= [|\rho_k|^2\cdot J_k^2(m)]_{k=0} + \\ &\quad + 2\sum_{k=1}^{n}|\rho_k|^2\cdot J_k^2(m), \end{aligned}$$

in which $J_k(m)$ is the first-type Bessel's function, of order k and subject m (index of modulation). The first term represents the power relative to the carrier and the sums of the terms of the series refer to the lateral lines. Coefficient 2 presupposes an identical contribution of the two lines of each pair of order k, and this derives from the fact that for a small $|\Delta f|f|$, the modulus of the filter's transfer function is symmetrical vis-a-vis the tuning frequency. In the expressions of [29], the subscripts k of the functions $|\rho|$, α, β, γ indicate that they are to calculated by putting into expression [17] for normalized reactance, of which all of them are a function, the value:

[30] $$(\Delta f)_k = kf_m\cdot 10^{-3} \qquad \text{(with } f_m \text{ in kHz, } f_o \text{ in MHz)},$$

in which k takes on, successively, all the whole-number values between 0 and n.

The sum of the power ratios [29] is equal to 1 when sums of the terms of the series are extended to number n of the pairs of lines that make up the signal (in theory, $n = \infty$); in practice, the calculation was done by putting into the computer program a "test" that interrupts the sums of the terms of the series for that value of n by which there results:

$$P_{RC}/P_1 + 2P_{R1}/P_1 + 2P_{R2}/P_1 + P_{RL}/P_1 \geq Q,$$

Q having been fixed as 0.9999; in this way, the 2n + 1 lines of the spectrum that contribute 99.99 percent to production of total power are taken into consideration. One notes that by putting into the expressions of [29] m = 0, the expressions of [27] are obtained again, keeping it in mind that $J_k(0) = 1$ for $k = 0$ and $J_k(0) = 0$ for $k \neq 0$.

The upper part of Table 2 presents the values of the powers calculated with both nonmodulated and modulated carrier, by menas of [27] and [29], for a frequency deviation $\delta f = \pm 75$ kHz and for a transmitter power $P_1 = 10$ kWatt at the frequency of 89 MHz (ring X).
In an analogous manner, by modulating transmitter 2 one can obtain the expressions of P_{RC}/P_2, P_{R1}/P_2, P_{R2}/P_2 amd P_{RL}/P_2. In this case, though, the sums of the terms of the series relative to the higher lines and to the lower lines with regard to the carrier must appear separately, because frequency f_2 of TX2 is on a side of the characteristic and the lines of the spectrum are treated in a dissymmetrical manner.

The lower part of Table 2 presents the values calculated for transmitter 2 at 89.9 of ring X with $P_2 = 10$ kW.

The total power dissipated in each cavity and in the absorption load is obtained as the sum of the corresponding powers dissipated by the two transmitters, and the sum of the voltages must be assumed as the maximum voltages.

It should be noted that for the TX2 one has both a negligible difference in the distribution of the powers as between the conditions of nonmodulated transmitter and modulated transmitter, and somewhat reduced losses of useful power (see section 9).

Once the value of the power for each cavity is known, it is easy to go back to the maximum currents and voltages on the internal elements, knowing the transformation ratio. For example, the voltage at the open end of the cavities C_1 and C_2 (Figure 24), relative to nonmodulated TX1 only, is:

$$V_A = \frac{\sqrt{P_{R1} \cdot r \cdot R_C}}{\sin (a\,\pi/2)} = 11847 \text{ volt.}$$

8. Resonant Cavities of the Filter

Once the structure of the cavities and the Q necessary for achieving the desired radioelectric characteristics are established, one goes on to determine their diameters. This subject was dealt with in sections 6 and 7 (Bibliography 6), and therefore only the essential part of it is reviewed here.

Table 2

TX1 (89 MHz)	Nonmodulated carrier f_1 (W)	Modulated carrier f_1 f_m = 1 kHz (W)	Modulated carrier f_1 f_m = 15 kHz (W)
P_{RC}	9,615.46	9,546.32	9,544.55
P_{R1}	98.00	108.22	108.17
P_{R2}	94.27	93.60	93.57
P_{RL}	$0.36 \cdot 10^{-3}$	49.07	51.30
Loss of useful power (dB)	- 0.17	- 0.20	- 0.20

TX2 (89.9 MHz)	Nonmodulated carrier f_2 (W)	Modulated carrier f_2 f_m = 1 kHz (W)	Modulated carrier f_2 f_m = 15 kHz (W)
P_{RC}	9,940.60	9,938.12	9,938.45
P_{R1}	0.34	0 35	0.35
P_{R2}	11.90	12.03	12.03
P_{RL}	34.90	36.12	36.11
Loss of useful power (dB)	- 0.026	- 0.027	- 0.027

the coefficient of quality for the coaxial resonator is:

[31] $Q = 4.17\sqrt{f/\rho_r} \cdot D \cdot \phi(D/d)$ (with f in MHz, D in mm)

in which D = inside diameter of the external conductor, d = diameter of the internal conductor, and ρ_r = resistivity as referred to that of copper.

The function $\phi(D/d)$ presents a maximum, of unitary value, for D/d = 3.6, corresponding to a characteristic impedance R_{cc} = 77 ohms.

The value furnished by [31] is the maximum obtainable with a coaxial line; in practice, lower values are obtained.

When the energy stored in the resonator's electromagnetic field remains constant, independently of the number i of dissipative elements, the real Q_o is obtained as a parallel of the Q's that there would be from inserting the i sources of loss one at a time:

[32] $Q_o = KQ$ with $K = 1/(1 + P_1/P + \ldots\ldots + P_i/P)$,

P being the power dissipated in the coaxial and P_i the powers dissipated by the i sources of added losses.

In the case being considered, it is possible to individuate principally two causes of loss (Figure 19): the short-circuit disc, which closes the cavity, into which all the maximum current I_o goes, and the strip contacts necessary for tuning the cavity.

The expressions of the loss ratios (formulas [25] and [26] of [as published] Bibliography 6) are referred to again; for the short-circuit disc:

[33] $P_1/P = 3.71 \cdot 10^{-6} \cdot f \cdot D \cdot \phi(D/d)$ (f in MHz, D in mm)

and for the strip contacts:

[34] $P_2/P = 26.66 \cdot 10^{-6} \cdot f \cdot L \cdot \cos^2\theta_o$ (f in MHz, L in mm)

in which θ_o is the distance in degrees between the selection field of the strip contacts and the shorshort-circuit plane and L is an equivalent line length that would give rise to the same losses as those due to the "fingers."

For the cavities of ring X one has: $\theta_o = 55.4°$ and L = 355 mm; $\phi(D/d) = 1$.

9. Distortions Introduced by the Combining Unit

In section 6 the necessity was pointed out of limiting the baseband distortions of the frequency-modulated signal transiting in the combining unit, especially in multiplex operation.

The problem of the distortions causes all the more concern the narrower the band of the circuits is, because of very close channeling, as is the case with the Mt Venda installation.

The RF signal outgoing from the filter is affected by distortions that alter its instantaneous amplitude and phase. The amplitude, which is no longer constant, varies in synchronism with the modulation of frequency by the effect of the limited channel width, giving rise to synchronous AM modulation, which is defined as the ratio between the difference and the sum of the maximum values V_M and minimum values V_m of the RF-signal envelope--that is:

[35] $$AM = \frac{V_M - V_m}{V_M + V_m} .$$

In reception, this distortion is eliminated by the limiters, while the phase distortions are transferred by the demodulator into the baseband signal.

For checking the distortions in the stereophonic signal, an original calculation procedure was used; it is described in Bibliography 8, and is applicable to any linear quadripole network whose transfer function is known. It calculates the distortions present in the A and B channels (left and right) after the RF signal modulated by a multiplex has transited through the filter.

In summary: the spectrum of the modulated signal, calculated by Fourier's transform, is multiplied by transfer function $H(\omega)$ of the filter, in the sense that each line of the spectrum is altered in amplitude and phase in relation to the modulus and phase of $H(\omega)$ at its frequency. At output from the filter, the antitransformed signal presents a variable instantaneous-amplitude envelope from which the synchronous AM is obtained, while the distortions are calculated on the basis of the demodulated signal, obtained by means of derivation of the instantaneous phase.

Several of the values calculated--for example, for channel 1 (89 MHz) in transit in ring X, applying power to channel A only with modulating frequency of 1 kHz and $\delta f = \pm 75$ kHz--are:

synchronous AM	0.93%
Linear diaphony	- 56.5 dB
Nonlinear diaphony	- 72.1 dB
Harmonic distortions	- 71.6 dB ,

which values are to be considered good.

Another procedure is mentioned, for evaluation of synchronous AM (Bibliography 9), that uses an approximate method but has the virtue of simplicity. It consists in assuming for V_M and V_m in [35] the maximum and minimum values taken on by the transfer function with variation of the frequency from the value f_o of the carrier to the values of the deflection peak $f_o \pm \delta f$. This procedure, called quasistationary approximation, furnishes synchronous-AM values approximated by defect. It has been observed experimentally that the approximation can be improved if the values $f_o \pm (\delta f + f_m)$ are considered as frequency extremes.

As regards reflected transmitter 2, the problem of distortions proves less important if the dimensioning of the circuit is appropriate.

Several differences between the characteristics of the TX1 in transit and those of the reflected TX2 of the same ring have already been noted (sections 7 and 6). For the latter, they are: lower losses, smaller differences in power distributioe between modulated and nonmodulated carriers, less group delay in the channel. Synchronous AM is also lower, being 0.12 percent for TX2 of ring X.

10. Auxiliary Circuits for Control of the Unit

The unit described is provided with a system of electronic circuits for the functions of monitoring, signaling, equipment protection and personnel safety.

10.1. Monitors

The monitoring circuits, situated in the instrument panel, furnishes readings of the direct and reflected power at the unit inputs for each transformer and at the output from the various rings, on lines A and B and on the artificial load (indicated by R_a in Figure 9).

In the same section there is monitoring of the reciprocal isolation of the transmitters between the gates 1 - 1' (Figure 8) for each ring, and switchable reading of the maximum temperature of the cavities.

Monitoring of the cavity-tuning conditions is furnished by reading of the power reflected by the cavities that goes back onto the absorption loads and by reading of the synchronous AM, which must be minimal in conditions of perfect tuning. These measurements too are switchable to each ring.

10.2. Signaling

Signaling is done with a number of LED's that constantly indicate the conditions of the circuit and signal any breakdowns. They are located partly in a group under the instrument panel and partly on the manual-switching frame. The former signal: power on in the transmitters; the position of the manual switches; presence of the protection systems. The lights on the manual-switch panel, though, permit switching only if the transmitters are not under power.

10.3 Equipment Protection

This consists in automatic action to shut down one or more transmitters whenever anomalies occur in the circuits powered by the unit, including the antenna. The parameters monitored by the protection systems are: maximum reflection on antenna lines A and B (shut-off of transmitters at the preestablished threshold); maximum power on artificial load R_a; maximum reentry onto absorption loads; maximum cavity temperature.

10.4. Personnel Safety

In addition to the usual safety provisions prescribed for every piece of equipment under tension, the unit and the manual-switching frame have been provided with a circuit for intervention in case of wrong or dangerous maneuver. This circuit reproduces, in direct current, all the possible runs of the RF power; only when all the runs of the RF are closed are the relays operated that enable the various transmitters to stay under power. Any dangerous maneuver is prevented, a little ahead of time, by the shut-off of the transmitter or transmitters transiting by way of the circuit section in question.

Acknowledgements

We cite: the essential contribution of Mr Giuseppe Novaira, who competently and skilfully carried out the entire cycle of measurements and the development of the entire radio circuit of the unit for Mt Venda, through its installation; Dr Francesco Rossi Doria, who efficiently supervised the construction and detailed installation of the auxiliary monitoring and safety circuits; Engineer Renato Orta, who on the occasion of this project did an original and rigorous study of the distortions of the stereophonic signal (Bibliography 8), filling a void in the technical literature on the subject; and the Radiofrequency Laboratory for its notable contribution to the working-out and construction of the protection and safety circuits and related electronics.

APPENDIX

A) The relations that link a sinusoidal magnitude v(t) of pulsation ω_o (carrier) with a generic function of time x(t), modulating, are considered to be known. It is recalled that in frequency modulation, a biunivocal correspondence is established

between x(t) and the instantaneous separation of the frequencies of v(t) in relation to that of the nonmodulated sinusoid. For the instantaeous pulsation, one has: $\omega_i(t) = \omega_o + Kx(t)$.

Keeping it in mind that the instantaneous pulsation is the derivative, with regard to time, of the instantaneous phase, in the particular case of sinusoidal modulation --that is, $x(t) = \cos \omega_m t$--one has:

[36] $$v(t) = A \sin[\omega_0 t + K \int x(t)\,dt = A \sin[\omega_0 t + m \sin \omega_m t]$$

in which $m = \delta f / f_m$ is the index of modulation with δf frequency deviation corresponding to the peak value of the separation of the instantaneous frequency, and f_m is the modulating frequency. Expanding in [1] the sin and cos terms of the subject $(m \cdot \sin \omega_m t)$, one has also:

[37] $$v(t) = A\left\{J_0(m) \sin \omega_0 t + \sum_{k=1}^{\infty} J_k(m)[\sin(\omega_0 + k\omega_m)t + (-1)^k \cdot \sin(\omega_0 - k\omega_m)t]\right\}$$

in which $J_k(m)$ is the first-type Bessel's function, of order k and subject m.

The total power associated with the signal v(t) is given by the sum of the powers associated with the individual lines.

The fraction of power P_Q transmitted in a channel with limited band $B_Q = 2pf_m$ is expressed by:

[38] $$P_Q = A^2 \sum_{k=-p}^{+p} J_k^2(m) = A^2 \cdot Q$$

with $Q < 1$ and p is the number of pairs of lines considered around the carrier; for $P = \infty$, $Q = 1$ results.

B) If the modulating signal is composed of the sum of two sinusoidal tones $x(t) = \cos \omega_1 t + \cos \omega_2 t$, one obtains analogously:

[39] $$v(t) = A \sin[\omega_o t + m_1 \sin \omega_1 t + m_2 \sin \omega_2 t]$$

with $m_1 = \delta f / f_1$ and $m_2 = \delta f / f_2$, which, expanded, can be written (Bibliography 7) as:

[40] $$v(t) = A \sum_{h=-\infty}^{+\infty} \sum_{k=-\infty}^{+\infty} J_h(m_1) \cdot J_k(m_2) \cdot \sin(\omega_0 + h\omega_1 + k\omega_2)t.$$

The fraction of power P_Q transmitted in a channel of limited band B_Q is:

[41] $$P_Q = A^2 \sum_{h=-p}^{+p} \sum_{k=-q}^{+q} [J_h(m_1) \cdot J_k(m_2)]^2 = A^2 Q$$

with the condition $-B_Q/2 \leq \pm h\omega_1 \pm k\omega_2 \leq B_Q/2$ and in which p and q are the maximum orders of the Bessel's functions corresponding to the lines contained in the band considered $B_Q = 2M\omega_2$ (with $\omega_2 > \omega_1$ and M positive integer). For $p = q = \infty$, $Q = 1$ results.

BIBLIOGRAPHY

1. Young, L., "The Analytical Equivalence of TEM-Mode Directional Couplers and Transmission-Line Stepped-Impedance Filters," PROC IEE, 110, February 1963, pp 275-281.

2. Matthaei, G., Young, L., and Jones, E., "Microwave Filters, Impedance-Matching Networks, and Coupling Structures," McGraw-Hill.

3. Chuck Y. Pon, "A Wide-Band 3-dB Hybrid Using Semi-Circular Coupled Cross-Section," THE MICROWAVE JOURNAL, October 1969, pp 81-85.

4. Pacini, G.P., "25-kW UHF Combining and Vestigial Filter," ELETTRONICA, No 1, 1963, pp 2-9.

5. Pacini, G.P., "Automatic Frequency Stabilization for Distributed-Constants Resonating Circuits by Means of a Mechanical-Hydraulic Device," ELETTRONICA E TELECOMUNICAZIONI, No 6, 1969, pp 210-212.

6. Pacini, G.P., "Design Method for Audio-Video Combining Filters," ELETTRONICA E TELECOMUNICAZIONI, Part 1: No 2, 1970, pp 54-64; Part 2: No 3, 1970, pp 106-114.

7. Black, H., "Modulation Theory," D. Van Nostrand Company, Inc.

8. Orta, R., "Distortion of Stereophonic Signal in Frequency-Modulation Transmissions," Technical report No 80-22-1, November 1980. RAI, Research Center, Turin.

9. Boccazi, F., and Luzzatto, G., "The Synchronous AM Problem in FM TV Transmitters," IEEE TRANSACTIONS ON BROADCASTING, Vol BC-15, No 3, September 1969.

11267
CSO: 5500/2309

ITALY

SILICON AVALANCHE PHOTODETECTOR FOR OPTICAL COMMUNICATIONS

Turin ELETTRONICA E TELECOMUNICAZIONI in Italian May-Jun 81 pp 116-124

[Article by M. Conti, M. De Padova and A. Modelli*]

[Text] Summary--Silicon avalanche photodetector for optical-fiber communications. This paper describes the implementation of a reach-through avalanche photodetector for optical-fiber communication systems with 0.8 to 1 μm wavelengths. This photodetector has an $n^+p\pi p^+$ silicon structure and has been developed using the planar technique. Particular attention has been devoted to dopant profile, diffusion technique, geometry and other factors for use optimization. Technological features (guard ring, channel stop, field plate, getter, passivation) made it possible to achieve very low dark current and noise and even lower than those typical of available photodetectors. Two different systems have been implemented: diffusions on top by side [as published] of the incident light and overturn position. This avalanche photodetector operates with voltages from 200 to 300 V and variable avalanche gain up to a value 100. The responsivity is between 0.55 and 0.65 A/W for the wavelength range from 0.8 to 0.9 μm. Besides, low capacitance allows this photodetector to be an excellent device for 34 Mbit/s communication systems.

1. Introduction

In optical-fiber communication systems, the incoming optical signal is converted into an electrical signal by a photodetector that must have adequate characteristics--that is, it must not introduce appreciable distortion in the incoming signal and must generate the least noise possible. The greater the noise, the greater the signal level needed to ensure satisfactory communication, and consequently, the shorter is the communication section achievable at equal transmission power.

The maximum performance characteristics in the 0.7-0.9 μm band are obtainablle with a silicon avalance photodetector (Bibliography 1). Such a photodetector has an internal gain, and in this way the noise input of the succeeding amplifier can be made negligible. In addition, because of the physical properties of silicon, the avalanche noise is intrinsically low. In this way, sensitivities even 10 dB higher than those obtained with a p-i-n photodetector can be achieved.

---

* Doctor of Engineering Mario Conti of the SGS-ATES [expansion unknown]; Dr Matteo De Padova of the CSELT [Telecommunications Research and Study Center]; Dr Alberto Modelli of the SGS-ATES.

Typescript received 2 March 1981.

Particularly interesting is the RAPD (Reach-through Avalanche Photo-Detector) structure, which can be developed with planar technology, gives responsivities only a little lower than the theoretical limit even with supply voltages of only 150-350 V --thus far lower than for the step-junction detectors (Bibliography 1)--and finally, has low dark current and high reliability. For these reasons, the avalanche photodetector designed and built at the SGS/ATES by the joint SGS/ATES-CSELT group is of this type, and is styled by the acronym OCPDA (Optical-Communication Photo-Detector-Avalanche). Below are reported the optimal-design and fabrication conditions for this device.

2. Operating Principles and Simulation

The cross section of the photodetector is represented in Figure 1. The active zone is the one between the two broken lines, and it is an $n^+p\pi p^+$ junction typical of the "reach-through" structure.

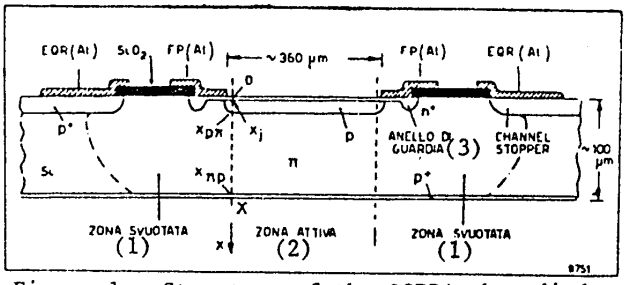

Figure 1. Structure of the OCPDA photodiode

Key:
1. Emptied zone 2. Active zone 3. Guard ring

Figure 2 represents: above, the profile of net concentration $N_d - N_a$ per cm^3 (N_d = concentration of donors, N_a = concentration of acceptors) along the lateral axis x (indicated also in Figure 1), and below, the profile of the electrical field E in the condition of voltage sufficiently high to empty the π region completely (Reach-Through situation: RT).

One notes that the maximum value of the electrical field ~2.5 - 3.10^5 V/cm is localized at the junction s_J, and that the multiplication of the carriers generated by the incident light is therefore concentrated there. There is also a far broader region, in which the electrical field is considerably lower and rather uniform, which functions as an absorption region for the incident photons and for collection of the charges generated by them.

All the regions present on the front are achieved with planar technology--that is, by obtaining, by photolithographic technique, adequate windows in a silicon-oxide state increased by heat oxidation, and by diffusing or implanting the appropriate doping agent through them (Figure 1).

Since the n^+ region is very thin, it is necessary to use an n^+ guard ring (deeper diffusion) that avoids problems of premature breakdowns and of metalization at the edge.

The "channel stopper" external p^+ ring serves to limit the emptied region laterally.

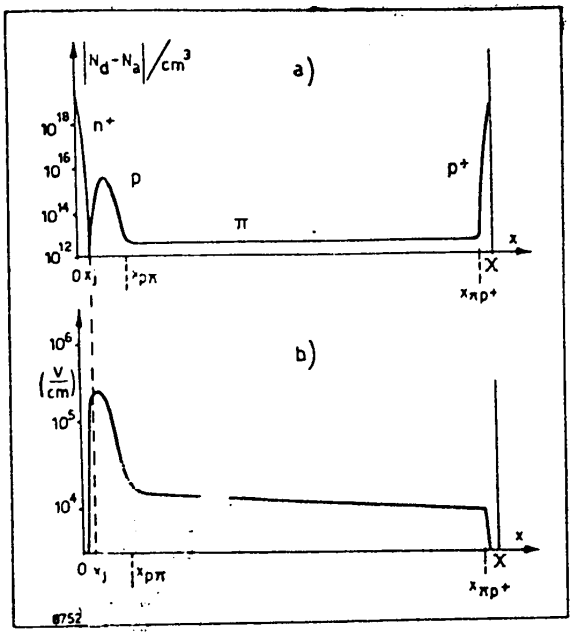

Figure 2. Profile of concentration a) and profile of electrical field b) along axis X (see Figure 1) in the active zone of the photodiode

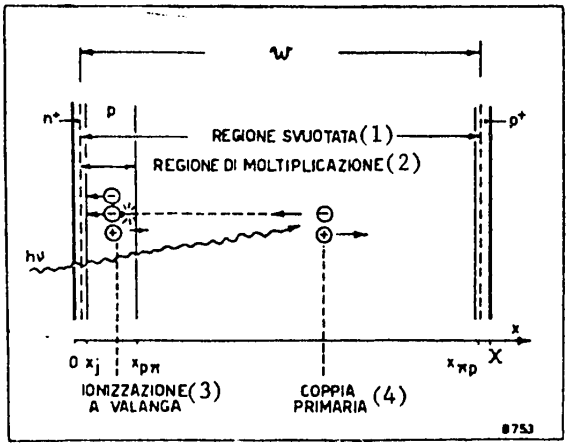

Figure 3. Diagram of the operating principle of the "Reach-through Avalanche Photo-Detector" (RAPD) photodiode

Key:
1. Emptied region
2. Multiplication region
3. Avalanche ionization
4. Primary pair

Metalization, in the classic planar structure with field electrode (FP = field Plate, Figure 1) and equipotential ring EQR (Figure 1), is useful in stabilizing the situation of the electrical field at the surface. In this way, surface breakdown phenomena are avoided and the leakage current is kept low and stable in time.

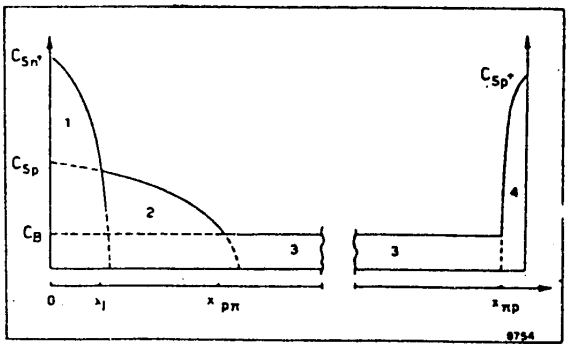

Figure 4. Concentration profiles used in digital simulation of the diffusion process (logarithmic scale for concentration). 1: profile of n^+ diffusion with surface concentration C_{Sn^+}; 2: profile of p diffusion with surface concentration C_{Sp}; 3: constant concentration C_B in the π zone; 4: profile of p^+ diffusion.

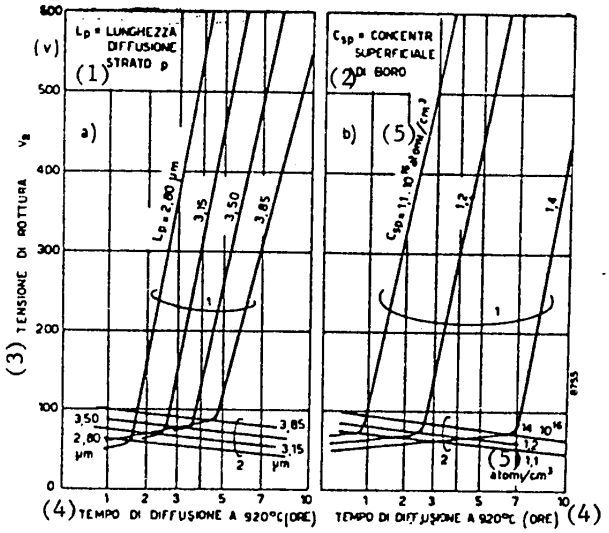

Figure 5. Simulation of the n^+ diffusion process: a) parameter of each curve diffusion length L_p [as published] of the p layer; b) parameter surface concentration C_{Sp} [as published] of the p layer.

Key:
1. L_p = diffusion length, p layer
2. C_{sp} = surface concentration of boron
3. Breakdown voltage
4. Diffusion time at 920°C (hours)
5. atoms per cm^3

The sensitive area of the device is circular, with diameter 360 µm, and its size was determined so as to limit the device's capacity as much as possible while permitting easy coupling to the optical telecommunications fiber, which, as is known, has an outside diameter of 120-200 µm.

When an electron-gap pair is generated by absorption of a photon, the electron, by effect of the electrical field, moves toward the n^+ region and passes through the high-field region situated at the junction x_j (Figure 3). In this region, the electrical field is such as to give it sufficient energy to ionize by impact--that is, to create an electron-gap pair, which in turn can produce another pair, and so on. Consequently, the current relative to a single photon becomes multiplied by a factor that depends on the electrical field and therefore on the voltage applied to the photodetector. The electrons are then collected by the n^+ region, while the gaps move toward the p^+ region and are collected there. This thin p^+ layer, in the rear of the chip (Figures 1 and 3), keeps the emptied region from reaching the rear surface and also makes good ohmic contact possible.

The structure of Figure 2, which has been studied in depth, has the particular characteristic that the avalanche multiplier effect, and therefore the gain of the photodiode, grow in a relatively slow manner with increase of the voltage applied.

The profile of reference impurities is shown in Figure 4.

The profile of the electrical field E(x) is calculated with Poisson's equation:

[1] $$\frac{d^2v}{dx^2} = \frac{\rho}{\varepsilon}$$

in which v = electrostatic potential, ε = dielectric constant, ρ = spatial charge assumed equal to the net concentration of doping agent--that is:

[2] $$\rho = q(N_d - N_a)$$

with q = charge of the electron.

Equation [1] is solved in a numerical manner by imposing the corresponding contour conditions at an applied reverse voltage $v = V_R$. A complication arises from the fact that the thickness x_d of the emptied region is not known beforehand. The calculation therefore proceeds by beginning with a zero emptying thickness and increasing it gradually until the required voltage V_R is reached.

The capacity per unit of surface of the photodiode is given by:

[3] $$c = \varepsilon/x_d.$$

The multiplication factor M, defined as the ratio between carriers collected for each photon absorbed, is given by the expression:

[4] $$M = \frac{\exp\left[-\int_0^w(\alpha_n - \alpha_p)\,dx\right]}{1 - \int_0^w \alpha_n \exp\left[-\int_0^x(\alpha_n - \alpha_p)\,dx'\right]dx}$$

in which:

[5] $$\alpha_n = \alpha_{n\infty} \exp(-b_n/E),\ \alpha_p = \alpha_{p\infty} \exp(-b_p/E).$$

The values of the coefficients valid for silicon (Bibliography 2) at ambient temperature are:

$\alpha_{n\infty} = 3.8 \cdot 10^6$ cm^{-1}, $\alpha_{p\infty} = 2.25 \cdot 10^7$ cm^{-1},
bn = $1.75 \cdot 10^6$ V/cm, bp = $3.26 \cdot 10^6$ V/cm.

Since α_n and α_p according to [5] depend on E, M proves to be an increasing function of V_R, and for a certain value $V_R = V_B$ tends to infinity (for $V_R > V_B$, it becomes negative). V_B obviously represents the breakdown voltage of the photodiode, which is therefore defined by the expression $M(V_B) = \infty$.

It is of particular interest for design purposes to analyze the influence on V_B of the net doping profile. It is strongly determined by the n^+ diffuse region, which must be regulated in such a way as to neutralize the correct quantity of acceptors introduced with the p diffusion. As will be explained later, this is achieved by depositing an appropriate quantity of n^+ doping agent (phosphorus) on the surface and raising the chip to 900-1,000 °C for a time t_n, so that the phosphorus diffuses in the chip with Gaussian profile whose characteristic length is $L_n = \sqrt{D_n t_n}$ in which D_n is the diffusivity of the phosphorus under the operating conditions. The final profile can be approximated by a distribution of acceptors with practically immobile Gaussian distribution from which one subtracts the distribution of donors, which depends on the heat treatment described.

With these premises, the voltage V_B was calculated in function of diffusion time t_n. The case of diffusion at 920 °C is represented in Figure 5a)b).

One notes that the curves of breakdown voltage in function of diffusion time are composed of two straight lines. In the first line, the breakdown voltage is lower than the voltage necessary for emptying the p zone and the breakdown voltage increases slowly. As soon as the n^+ diffusion has sufficiently compensated for the p diffusion, the breakdown voltage begins to increase far more rapidly with diffusion time.

For the purposes of study of the process, it has been interesting to study how the form of the diffusion curves varies with the variation of two initial parameters, which are the length L of diffusion of the p layer and its total dose. The curves of Figure 5a) were calculated for a constant total boron dose Q_p by varying its diffusion length L_p that appears as a parameter. Figure 5b), on the other hand, corresponds to the case of a p diffusion with constant diffusion length L_p but with variable total dose Q_p; in this case, C_{sp} is the surface concentration of boron, assumed as a parameter. The curves indicated by 1 represent the breakdown voltage V_B, and those indicated by 2 represent the voltage at which emptying of the π region begins.

Comparing Figures 5a) and b), one notes that the process is far more critical with regard to the predepositing of boron rather than with regard to the diffusion of boron. Indeed, going from a boron surface concentration of $1.1 \cdot 10^{16}$ to $1.2 \cdot 10^{16}$ atoms per cm^2, a good 1 hr 30' shift of the rediffusion curves at 920° is obtained. This shows that very high uniformity is necessary in the boron dose deposited in order to avoid localized breakdowns.

3. Fabrication

As the starting material for making these avalanche photodiodes (APD), Float Zone silicon chips of 2" diameter, with resistivity of 2,000-4,000 ohms·cm and orientation (111) are used. The high resistivity, obtainable only with material of "detec-

tor" class, is indispensable for achieving empty regions more than a hundred microns thick with breakdown voltages lower than 350 V.

After the initial polishing and oxidation, the first two processes are carried out: the making of the n^+ guard ring and of the p^+ "channel stopper," achieved with planar diffusion in an atmosphere of, respectively, phosphorus (from $POCl_3$) and boron (from BN).

As regards the p deposition, after many tests carried out with the traditional deposition process (predepositing with BN chips followed by a double "steam leach"), the necessity of having greater uniformity emerged and it was decided to go over to deposition by ionic implantation. This method does indeed make it possible to regulate the dose deposited--which in our case is about $4 \cdot 10^{12}$ atoms per cm^2--with great precision.

A measuring process that makes it possible to check accurately the dose deposited has also been developed. It uses the four-points method (Bibliography 3) and makes it possible to have a direct check on the dose implanted. It is essential for the dose to fall within very narrow limits; indeed, if there is a deficiency of boron, the chips go into breakdown at excessively high voltages, and if it is too abundant, it is necessary to rediffuse the n^+ for too long a time, which reduces quantic efficiency in case of illumination from the front.

After implantation of boron, the chip is raised to 1,200° C in a controlled atmosphere for several hours so as to achieve rather deep diffusion, with characteristic length $\sqrt{D_p t_p} = 1.8$ μm.

The chip is then brought to a thickness of 120 μm by means of lapping and chemical attack on the rear face. An implantation of about 10^{14} atoms/cm^2 of boron on the rear constitutes the rear p^+ region.

Finally, the chip is treated in a phosphorus ($POCl_3$) atmosphere at 920° for a suitable time so as to cause penetration of the phosphorus previously deposited on the front and to achieve the required profile of acceptors in the p region. The treatment takes place in a phosphorus atmosphere, and in this way a "gettering" effect (Bibliography 4) is obtained which is useful for eliminating microdefects in the material and consequent causes of premature breakdowns. The cooling cycle, which has to be a very slow one, is also very important.

4. Metalization

The two types of arrangement that have been made and evaluated are represented in Figure 6. In the first, a), light falls on the photodetector from the n^+ diffused region, or from the front, while in the second case, b), it falls from the p^+ region, or from the rear.

The first arrangement is of a type conventional for integrated-circuits technology. The metalization on the front (FP field electrode of Figure 1 and equipotential ring EQR of Figure 1) is of aluminum, while that on the rear it is of nickel-chromium. An antireflectant layer of Si_3N_4 or SiO is then deposited, as described later on.

In the second arrangement (Figure 6b), it is necessary to make a metallic "cushion" of sufficient thickness to keep the alloy from making contact with the equipotential

ring during the operation of soldering the plate to the bottom, causing a short circuit of the diode.

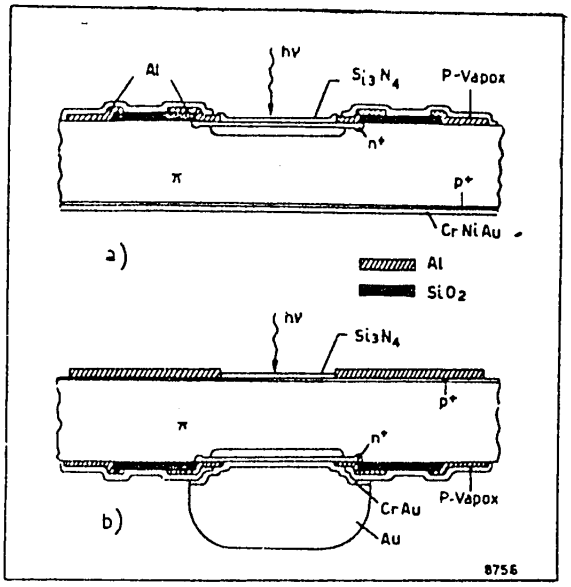

Figure 6. Section of two OCPDA photodiodes with different metalization: a) for front illumination; b) for rear illumination.

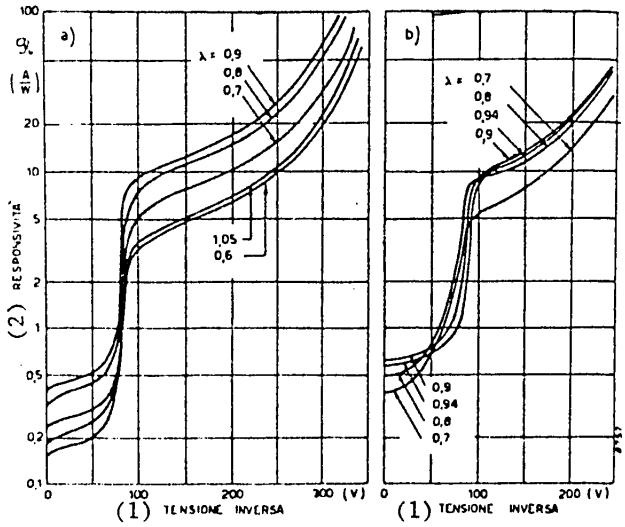

Figure 7. Responsivity in function of polarization voltage for various values of incident wavelength: photodetector illuminated from the side of a) p^+ diffusion; b) n^+ diffusion.

Key:
1. Reverse voltage
2. Responsivity

For this purpose, a "cushion" of gold, about 50 μm thick, is made from galvanic growth, starting from a layer of gold-chromium evaporated over the aluminum metalization and delineated by photolithography. At the same time, the metalization on the p^+ side is done, aligned with the preceding and achieved by evaporation of aluminum. In this case also, an antireflectant layer of suitable material and thickness is deposited.

The plate is then soldered onto a type TO-5 container with ceramic mount. In this way, both cathode and anode are separated from the metal case, and the diode's satellite capacitances can therefore be reduced or eliminated.

Closed photodiodes are then made, with cap with transparent window of glass or with optical fiber incorporated. This last-named version is of particular interest for optical-fiber communications, since in such case the connection to the line fiber is by a simple aligned auto joint and does not require an additional operation.

5. Performance Characteristics of the Avalanche Photodetector

5.1 Responsivity

The responsivity of an APD detector is defined as the ratio between the detected current and the incident photonic power at a given gain and wavelength.

In the case of a detector with given gain M, it can be expressed as the result of the following processes: reflection at the surface, absorption in the frontal region, conversion of phontons into electron-gap pairs, and internal multiplication.

a) Reflection

Reflection of light at the surface of the diode can be reduced if it is covered with a layer of antireflectant material. It has been demonstrated (Bibliography 5) that if this antireflectant layer with refraction index n_2 has the thickness $d = \lambda/4n_2$ (λ = wavelength of the incident radiation), the reflectivity has the value:

[6] $$R = \left(\frac{n_3 n_1 - n_2^2}{n_3 n_1 + n_2^2}\right)$$

in which n_1 is the refraction index of the external space and n_3 is that of the silicon. As emerges from [6], reflection R can be minimized if n_2 is the geometric mean between n_1 and n_3.

For $n_1 = 1$ (air, vacuum), and since for $\lambda = 0.7 - 1$ μm for silicon one has $n_3 = 3.5 - 3.7$, then in order to obtain $R = \sim 0$, $n_2 \sim 1.9$ is necessary. Silicon nitride (Si_3N_4) and silicon oxide (SiO) have a refraction index close to that value.

b) Absorption in the Frontal Region

On the surface of the photodetector there is always a semiconductor layer (for example, n^+, Figures 1 and 3) that absorbs photons without contributing to responsivity. Given α as this layer's coefficient of absorption and w_s as its thickness, the fraction of luminous energy transmitted is:

$$\exp(-\alpha w_s).$$

It is obviously necessary to reduce w_s to the minimum, given that α depends on the material used and is a function of the wavelength λ employed.

c) Conversion

The photons that reach the emptied region of thickness w (Figure 3) are converted into electron-gap pairs. If the material is very pure, as is the "float zone" silicon generally used, the parasite absorption phenomena are negligible and the number of pairs created equals that of the photons absorbed.

Given P_o as the photon power entering into the emptied region, the generation of pairs is given by:

$$g(x) = \frac{\lambda}{hc}\left|\frac{dP(x)}{dx}\right| = \frac{\lambda\alpha}{hc} P_o \exp(-\alpha x)$$

in which h = Planck's constant and c = speed of light.

The current I produced by photon power P_o therefore has the value:

$$I = q\int_0^w g(x)\,dx = \frac{qP_o\lambda}{hc}[1 - \exp(-\alpha w)]$$

in which q = electron charge.

In this expression, the component of photons reflected by the rear surface has not been taken into consideration.

The total respoonsivity is the product of the factors considered and therefore has the value:

[7] $$\mathcal{R}(M, \lambda) = \frac{q\lambda}{hc}(1 - R) M \exp(-\alpha w_s) [1 - \exp(-\alpha w)]$$

in which M is given by [4].

[7] is valid for a photodetector, such as the one considered, made with a homojunction; it makes it possible to study the influence of α--which, as was said, depends on λ--on responsivity $\mathcal{R}$.

In silicon, α is large at short wavelengths, and $\mathcal{R}$ is therefore limited by the term $\exp(-w_s)$. With increase of λ, α decreases rapidly, and this term therefore tends toward 1; but the bracketed term, which, for α tending toward zero, also tends toward zero, becomes decisive. It is therefore important to use the biggest possible collection thicknesses w. This has a negative effect on response time, as will be shown farther on.

In Figures 7a) and b), the curves of responsivity $\mathcal{R}$ are presented in function of the reverse voltage applied for various wavelengths, for APD's illuminated both from the p^+ side and from the n^+ side.

Measurement was done by illuminating the detector with monochromatic light of known intensity, calibration having first been done with a rated EG & G radiometer. The current generated by the APD is amplified by an operational amplifier and recorded by a logarithmic recorder in function of the voltage applied. Gain M is evaluated as the ratio between the light current at the voltage involved and that of a p-i-n detector built with the same technology.

One notes that $\mathcal{R}$ (Figure 7a) is an increasing function of the voltage applied and repeats the course of M, which in fact appears in expression [7].

An abrupt increase occurs for V $\simeq$ 80-90 V--the voltage at which the reach-through situation appears. For lower voltages, $\mathcal{R}$ is that of a p-i-n diode, while with higher voltages it is much greater.

The case of illumination from the n^+ side (Figure 7b) is similar to the preceding, except that one notes that the falloff of $\mathcal{R}$ at the short wavelengths is greater.

Comparison is given in Figure 8, in which the high-gain responsivities of both the p^+ APD and the n^+ APD are presented. It can be noted that for high wavelengths (0.9 - 1 m), the OCPDA devices have better responsivity than the best devices available on the market. This is explained by their having a rather thick intrinsic zone ($\simeq$ 120 μm). At the short wavelengths, the responsivity of the n^+ 1 detector is lower than that of the p^+ type; this is because of the fact that a part of the radiation is absorbed by the front region n^+. The n^+ 2 specimen, though, in which the n^+ diffusion is less heavy, has high responsivity even at this wavelength.

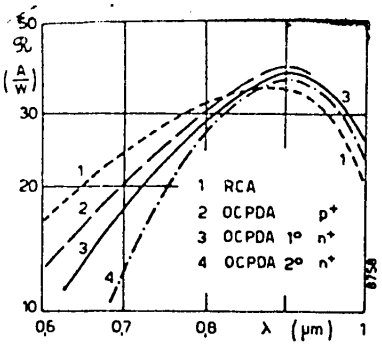

Figure 8. Spectral response of several photodiodes illuminated from the p^+ or n^+ side for a multiplication value M = 60.

If the results presented in Figure 8 are compared with those calculated with [7½, it is verified that experimental $\mathcal{R}$ is only slightly less than the theoretical value in the field 0.7 - 0.9 μm--that is, in one of the areas of greatest interest for optical communications.

5.2 Capacity

The capacity associated with the detector has negative effects on both speed of response and noise, contributing to an increase in amplifier noise (see below). It is therefore important to limit it as much as possible.

It consists of three components:

--capacity associated with the central active region and with the n^+ guard-ring region; it is that of a flat condenser, and for high voltages therefore tends toward vacuum value (Bibliography 3);

--capacity relative to the lateral cylindrical region and to the field electrode FP; at operating voltage, though, these are negligible;

--capacity due to the bottom; this capacity is minimized by mounting the detector on an insulating plate in such a way that no terminal of it is in electrical contact with the bottom; with this mounting, the parasite capacity can be reduced to about half what it would be with direct mounting on the bottom (0.3 as against 0.6 pF).

The capacity-voltage curve is given in Figure 9. At the voltage of 70-90 V, one notes an abrupt dropoff of capacity, which is due to arriving at the reach-through situation. For lower voltages one observes a second "hump" that is due to stabilization of the emptying situation in the semiconductor under the field electrode.

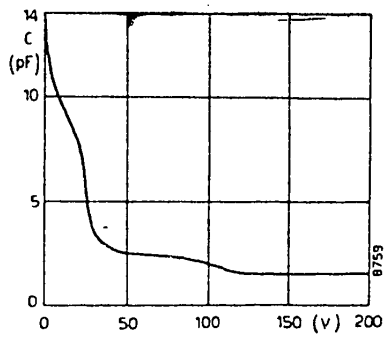

Figure 9. Characteristic of capacity in function of the polarization voltage of an OCPDA photodiode

In the last analysis, there is little difference in capacity in operating conditions in the two situations, n^+ and p^+; its value is 1.5 and 1.8 pF in connection with insulated bottom and with grounded bottom.

5.3 Speed of Response

The photogenerated charges pass through the w region at a speed v that depends on the electrical field present in it. As is known, with silicon it is proportionate, with low fields, to the electrical field in accordance with a coefficient of proportionality μ called mobility. But when the electrical field becomes high, on the order of 10^4 V/cm and above, the speed tends toward a saturation value v_s on the order of 10^7 cm/s. There is also a second cause of delay: the time needed by the avalanche to stabilize (Bibliography 1). But it is important only in devices that are very fast and not thick, such as the present ones, in which high responsivity is required for $\lambda = 0.8 - 0.9$ μm.

Transit time can be calculated with the expression $t_t = 0.8$ w/v; it conditions the photodetector's intrinsic cut-off frequency, given by the expression:

$$f_{3dB} = 0.4 \text{ v/w} = 0.5/t_t.$$

In order to keep the cut-off frequency high, a high v must be achieved, in view of the fact that w cannot be too small, which would reduce responsivity. This is done by keeping the electrical field high in the w region, and therefore a part of the voltage applied has the purpose of achieving this electrical field.

The pulse response of this photodetector is presented in Figure 10.

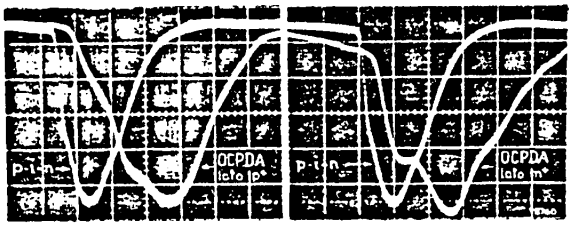

Figure 10. Oscillograms of the response of OCPDA photodiodes subjected to a light pulse. The response of a fast p-i-n diode is given for comparison. Axis of the abscissas: 1 ns/div.

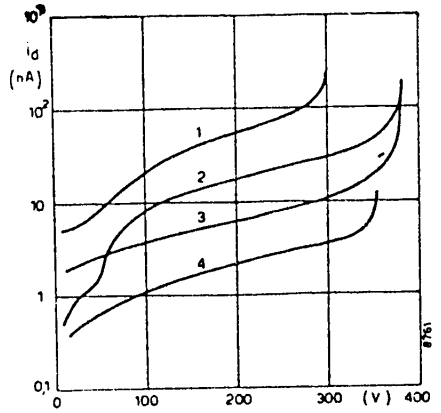

Figure 11. Inverse characteristics in dark of four OCPDA diodes

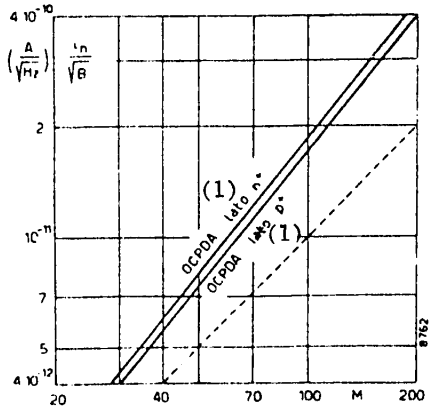

Figure 12. Spectral density of noise current in function of multiplication factor M (the broken line shows, for comparison, a course proportionate to M).

Key:
1. Side

The light pulse is generated by a type-C 30025 laser and has a width t* that is measured by a fast p-i-n detector with a rise time $t_S \lesssim 0.35$ ns.

Response time with impulse excitation is obtained by subtracting time t* from the measured value t_m with the expression:

$$t = \sqrt{t_{m2} - t^{*2}}.$$

One thus obtains values of about 2 ns and 3 ns, respectively, for detectors of type p^+ and n^+. The difference, and also the rather different form of the pulse detected, are due to the fact that in the first type, multiplication is rather uniform for all the photogenerated carriers, while such is not the case with the n^+.

The times given are entirely satisfactory for 34-Mb/s PCM systems and also for higher frequencies. They can be further reduced by reducing the thickness of the detector.

5.4 Noise

As was said in the introduction, it is important for the detector-amplifier system to introduce very low noise, so as not to deteriorate the incoming information. The lower the noise, the lower the optical power necessary to ensure detection of preestablished quality (signal-to-noise ratio, error rate, etc), and therefore, the longer the section that can be constructed for a given transmission power. Let us review the various causes of noise introduced by the detector and evaluate their contribution to total noise.

a) Quantic Noise

With an optical power P_o there is associated a flux of n electrons (that flow independently) in which $n = \eta P_o/h\nu$) in which η quantic efficiency of the detector, h = Planck's constant, ν = frequency of the radiation. The fluctuation of these electrons gives rise to a "shot" noise current whose mean quadratic value is given by:

[8] $\overline{i_{s2}} = 2qBI_p$ with $I_p = \eta qn$ = photogenerated current for M = 1, and B = pass band.

b) Avalanche Noise

In the avalanche process, the individual light pulses are multiplied in accordance with a stochastic process, and the noise is therefore greater than what would be calculable if only the individual packets $I_p \cdot M$ were considered; this is taken into account by means of the coefficient F, that is called the "excess noise factor." The noise current is therefore given by:

[9] $$\overline{i_{n2}} = 2qFBI_pM^2$$

in which:

[10] $$F = M\left(1 - \frac{(1-k)(M-1)^2}{M^2}\right)$$

with $k = \alpha_p/\alpha_n$

in which α_p and α_n are, respectively, the coefficients of ionization for the gaps and for the electrons. F therefore proves to be an increasing function of multiplication factor M. Moreover, the lower k is, the smaller F is; it is therefore good

for the primary charges (electrons in silicon) to be those with the highest coefficient of ionization. This explains the choice of the $n^+p\pi p^+$ structure for this photodetector.

From the expressions [5] of α_n and α_p it is deduced that ks smaller as the avalanche electrical field is lower. However, low fields require considerable avalanche thicknesses and therefore high polarization voltages.

In the case in question, a value of k = 0.02 was obtained, which entails a rather small value of F in operational multiplications.

c) Dark Current

The detector's reverse dark current also involves a fluctuation and therefore noise: it is composed of a surface term I_s and a "bulk" or mass term I_b. They are given by:

$$I_s = qn_i v_r A_s, \qquad I_b = \frac{L}{2} q \frac{n_i}{\tau} A_j w$$

in which: n_i = intrinsic concentration, v_r = speed of surface recombination, τ = average life in vacuum in silicon, and A_s and A_j are the surface area not involved in the multiplication and the surface area of the junction (Bibliography 3).

The dark noise current is calculated with the Shot-effect formula, and is:

[11] $$\overline{i^2} = 2qB\ (I_s + I_b M^2 F).$$

In Figure 11 are given the reverse-dark-current curves for several OCPDA diodes in function of applied voltage.

d) Noise Due to Amplifier

The photodetector is closed on a resistance R_L which is the amplifier's input resistance: a thermal noise is associated with it. In addition, the amplifier is the site of noise that can be represented by increasing the noise produced by R_L in accordance with the coefficient F_A (noise factor of the amplifier). The noise current of the amplifier therefore proves to be:

[12] $$i_A = \frac{4KTB}{R_L}\left[1 + F_A\left(1 + \frac{\omega^2 R_L^2 C^2}{3}\right)\right]$$

in which K = Boltzman's constant, T = absolute temperature, C = total capacity at amplifier input, and $\omega = 2\pi f$ is the angular frequency of the signal.

Since the signal power associated with P_o is given by $\frac{1}{2}\left(\eta \frac{q\lambda}{hc} P_o M\right)^2$, the overall ratio S/N between the signal and the noise is given by:

[13] $$\frac{S}{N} = \frac{\frac{1}{2}\left(\eta \frac{q\lambda}{hc} P_o M\right)^2}{2qB\left[I_s + \left(I_b + \eta \frac{qP_o}{h\nu}\right) M^2 F\right] + \frac{4KTB}{R_L}\left[1 + F_A\left(1 + \frac{\omega^2 R_L^2 C^2}{3}\right)\right]}.$$

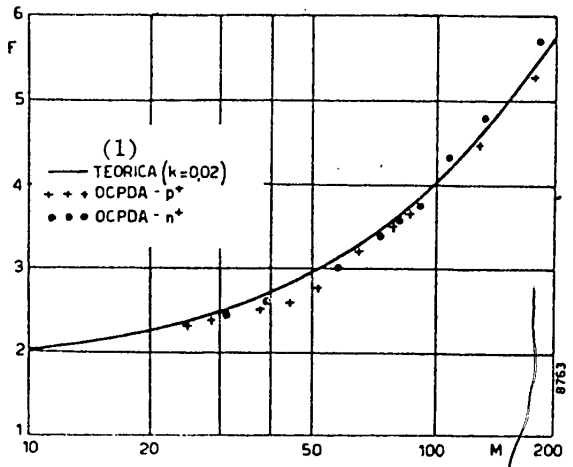

Figure 13. Course of excess noise factor F with increase of M: +++ diode illuminated from the p^+ diffusion side; ··· diode illuminated from the n^+ side

Key:
1. Theoretical

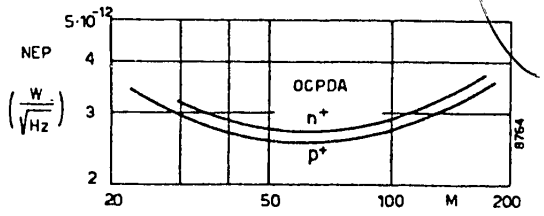

Figure 14. Noise Equivalent Power in function of M

[13] expresses quantitatively the dependence of the signal-to-noise ratio on the various parameters of the detector and of the amplifier. We find the fact that with the presence as denominator of a term not dependent on M, S/N initially increases with the increase of M. Beyond a certain value, though, the tendency reverses, since the first term--in which, because of the presence of F, dependence on M is greater than in the numerator--becomes predominant as denominator.

Thus there exists an optimal value of M that optimizes the S/N ratio; to it corresponds the situation in which the two quantities to be added to the denominator are about equal. In these conditions, the maximum S/N value depends on the input-signal level P_o, on $1/R_L$, on F (factor intrinsic to the detector) and on the amplifier noise factor F_A, as well as on the total capacity in parallel to the detector C.

Measurement of noise was done by sending to the photodetector an optical power signal equal to 40 nW, obtained from an LED HRED 956 L emitting at 0.9 μm. The response was registered by a transimpedance amplifier with very low noise and was read with a voltmeter of true effective value.

With variation of the photodiode polarization voltage and therefore of multiplication M, the noise voltage was read, both with illuminated diode (V_L) and with diode

in dark (V_B). Subtracting the effective values, one obtains the value V_n related to the photonic noise--that is:

$$\overline{V}_n = \sqrt{V^2_L - V^2_B} \ ;$$

This value, divided by the amplifier's reaction resistance, provides the value of noise current i_n given by [9].

The course of i_n in function of M is represented in Figure 12; it can be noted that i_n increases faster than M. One can then deduce also the "excess noise" factor F given by [10].

In Figure 13 are given the F(M) curves for devices illuminated both from the p^+ diffsuion side and from the n^+ diffusion side. The experimental results coincide very well with the theoretical curve deduced from [10] and drawn in the figure for $k = 0.02$. This value is among the lowest reported in the literature, and it has been possible to achieve it only with appropriate geometry and careful technology. The commercially available devices have slightly higher k values: typically, $k = \sim 0.025$.

Another notable datum useful for expressing the good quality of the detector is the NEP (Noise Equivalent Power), defined as the incident-optical-power value necessary in order to have a unitary signal-to-noise ratio (S/N = 1); it proves to be:

$$NEP = \frac{i_n}{\mathcal{R}\sqrt{B}}$$

The value of NEP is derived from the preceding measurements of i_n given by [9] and of $\mathcal{R}$ given by [7]. The typical course of OPCDA photodetectors is given in Figure 14; it presents a minimum for values of M around 60 - 70. This value of the multiplication factor M is therefore the one that optimizes the S/N ratio of the detector system.

6. Conclusions

The optimization criteria, the fabrication process, and the electro-optical performance characteristics of the OCPDA avalanche photodiode designed to be used in optical fiber systems with wavelength between 0.8 and 1 μm are described.

The $n^+p\pi p^+$ planar structure with channel stopper and other technological expedients has made it possible to obtain devices with high multiplication and very low dark current.

Two possible arrangements of the diode were constructed and studied: diffusion from the incident-light side and in the reversed position. For the wavelength involved, 0.8 - 0.9 μm, a small difference in responsivity values was observed; as regards noise also, it was seen that it decreases only slightly with illumination of the diode from the p^+ side. The structure with illumination from the p^+ side (Figure 6b) therefore does not seem so much superior to the other as to justify the necessary technological complications, except for very advanced applications.

In conclusion, the OCPDA device made by the SGS/ATES-CSELT group presents characteristics comparable to those of the competition, and in some respects superior, as regards dark currents and noise.

Acknowledgements

The authors wish to thank Dr G. Randone for the discussions with him and Messrs L. Gandolfi, G Vento and A. Destro for their contributions to the construction of the devices.

BIBLIOGRAPHY

1. Webb, P., McIntyre, R.J., and Conradi, J., RCA REVIEW, 35, 1974, p 235.

2. Sze, S.M., and Gibbons, G., APPL PHYS LETT, 8, 1966, p 111.

3. Grove, A.S., "Fisica e Tecnologia dei Dispositivi a Semiconduttore" [Physics and Technology of Semiconductor Devices], F. Angeli Ed., Milano, 1978, p 90.

4. Ibid, p 249.

5. Born, M., and Wolf, E., "Principles of Optics," Pergamon Press, 1975, p 61.

6. Philipp, H.R., and Taft, E.A., PHYS REV, 120, 1960, p 37.

7. McIntyre, R.J., IEEE TRANS EL DEVICES, ED-13, 1966, p 164.

11267
CSO: 5500/2310

END